nature plants

Article

https://doi.org/10.1038/s41477-023-01419-8

A redundant transcription factor network steers spatiotemporal *Arabidopsis* triterpene synthesis

Received: 5 October 2022

Accepted: 14 April 2023

Published online: 15 May 2023

Check for updates

Trang Hieu Nguyen[1,2], Louis Thiers[1,2,3], Alex Van Moerkercke[1,2], Yuechen Bai[1,2,12], Patricia Fernández-Calvo[1,2,13,14], Max Minne[1,2], Thomas Depuydt[1,2], Maite Colinas[1,2,15], Kevin Verstaen[4,5], Gert Van Isterdael[6,7], Hans-Wilhelm Nützmann[8,9], Anne Osbourn[8], Yvan Saeys[5,10], Bert De Rybel[1,2], Klaas Vandepoele[1,2,11], Andrés Ritter[1,2,16] & Alain Goossens[1,2,16]

Plant specialized metabolites modulate developmental and ecological functions and comprise many therapeutic and other high-value compounds. However, the mechanisms determining their cell-specific expression remain unknown. Here we describe the transcriptional regulatory network that underlies cell-specific biosynthesis of triterpenes in *Arabidopsis thaliana* root tips. Expression of thalianol and marneral biosynthesis pathway genes depends on the phytohormone jasmonate and is limited to outer tissues. We show that this is promoted by the activity of redundant bHLH-type transcription factors from two distinct clades and coactivated by homeodomain factors. Conversely, the DOF-type transcription factor DAG1 and other regulators prevent expression of the triterpene pathway genes in inner tissues. We thus show how precise expression of triterpene biosynthesis genes is determined by a robust network of transactivators, coactivators and counteracting repressors.

Plants have the ability to synthesize a wide range of specialized metabolites with important roles in growth, development, defence and/or interactions with the environment[1,2]. Accordingly, together with the structural variety of the metabolites, complex regulatory networks have coevolved to ensure correct spatiotemporal activation of the corresponding biosynthetic pathway[2,3]. Although several regulators involved in the hormone- or stress-mediated induction of specialized metabolism have been identified in the past[4], the cell-specific regulation of specialized metabolic pathways remains elusive. For instance, some terpenes (one of the major classes of plant specialized

[1]Department of Plant Biotechnology and Bioinformatics, Ghent University, Ghent, Belgium. [2]VIB Center for Plant Systems Biology, Ghent, Belgium. [3]Plant Sciences Unit, Flanders Research Institute for Agriculture, Fisheries and Food (ILVO), Melle, Belgium. [4]VIB Single Cell Core, Ghent-Leuven, Belgium. [5]VIB Center for Inflammation Research, Data Mining and Modelling for Biomedicine, Ghent, Belgium. [6]VIB Flow Core, VIB Center for Inflammation Research, Ghent, Belgium. [7]Department of Biomedical Molecular Biology, Ghent University, Ghent, Belgium. [8]Department of Biochemistry and Metabolism, John Innes Centre, Norwich, UK. [9]Department of Biology and Biochemistry, The Milner Centre for Evolution, University of Bath, Bath, UK. [10]Department of Applied Mathematics, Computer Science and Statistics, Ghent University, Ghent, Belgium. [11]Bioinformatics Institute Ghent, Ghent University, Ghent, Belgium. [12]Present address: School of Life Sciences, Fudan University, Shanghai, P.R. China. [13]Present address: Misión Biolóxica de Galicia, CSIC, Pontevedra, Spain. [14]Present address: Centro de Biotecnología y Genómica de Plantas, Universidad Politécnica de Madrid (UPM)-Instituto Nacional de Investigación y Tecnología Agraria y Alimentaria (INIA), Campus Montegancedo UPM, Madrid, Spain. [15]Present address: Department of Natural Product Biosynthesis, Max Planck Institute for Chemical Ecology, Jena, Germany. [16]These authors jointly supervised this work: Andrés Ritter, Alain Goossens. e-mail: alain.goossens@psb.vib-ugent.be

metabolites)[5] can accumulate constitutively, while the production of others is (transiently) induced by a variety of developmental or environmental signals, often in association with biotic interactions and in a tissue-specific manner[6–8]. The model plant *Arabidopsis thaliana* (Arabidopsis) synthesizes several types of terpene compound[5,9,10], such as triterpenes that are built from the general precursor oxidosqualene through the action of triterpene synthases (TTSs) as the first committed step. The Arabidopsis genome possesses five TTSs organized in 'operon-like' biosynthetic gene clusters (BGCs), from which the thalianol and marneral BGCs have been characterized best (Supplementary Fig. 1)[11–14]. These BGCs are predominantly expressed in roots[7,11,12], and their expression results in the accumulation and/or secretion of root triterpenes, such as various thalianol derivatives that selectively modulate Arabidopsis root growth/development and the recruitment of the Arabidopsis root microbiota[7,15]. The marneral and thalianol BGCs are present in transcriptionally active chromosomal sites in roots and are localized to heterochromatic chromosomal domains when silenced in leaves[13], and the involvement of localized chromatin modifications in their regulation has been reported[13,14]. We recently revealed that jasmonate (JA) activates gene expression and increases metabolite accumulation of triterpenes from the thalianol pathway[15]. JA is a conserved phytohormone, widely renowned for its elicitor action in the production of a wide range of plant specialized metabolites[4,16,17]. In the absence of JA, the signalling pathway is repressed by a protein corepressor complex composed of the JASMONATE ZIM-DOMAIN (JAZ), the NOVEL INTERACTOR OF JAZ and TOPLESS proteins, which binds to specific transcription factors (TFs) to impede the JA response[18–21]. Upon stress, JA is synthesized in its bioactive form, JA-Ile, which is perceived by a coreceptor complex composed of the CORONATINE INSENSITIVE 1 (COI1) F-box protein that associates with CUL1, Rbx1 and Skp1-like proteins to assemble the SCF^{COI1} ubiquitin-ligase complex[21–23]. The SCF^{COI1} complex subsequently ubiquitinates the JAZ proteins, resulting in their proteasomal degradation and thereby releasing the inhibited TFs[17,19,21,24]. Despite this knowledge and the central role of the Arabidopsis triterpenes in metabolic regulation, TFs acting on the Arabidopsis triterpene BGCs have not been identified yet. Here we reveal a robust transcriptional gene regulatory network that determines the cell-specific and JA-inducible expression of triterpene biosynthesis genes in Arabidopsis root tips, thereby exposing a fundamental regulatory mechanism of specialized metabolite production in plants.

Results

Expression of genes in the triterpene BGCs is root-cell specific and JA inducible

Our previous data, together with available transcriptome datasets of the JA repressor mutants *ninja* and *jazQ*, indicated that JA activates expression of marneral and thalianol BGCs[15,25,26]. We first corroborated these data in roots of 12-day-old Arabidopsis Col-0 wild-type (wt) and *coi1-1* mutant seedlings treated either with mock or 50 µM JA for 6 h (Fig. 1a). Expression of genes from both the thalianol BGC (that is *THAS, THAH* and *THAO*) and the marneral BGC (that is *MRN1, CYP705A12* and *MRO*) was strongly induced by JA treatment in wt roots, whereas this effect was abolished or significantly lowered in the *coi1-1* background (Fig. 1a). Correspondingly, roots of JA-treated wt seedlings accumulated significantly higher amounts of thalianol compared with mock-treated plants (Fig. 1b). In the *coi1-16* mutant, the JA-mediated increase in thalianol content was largely reduced; no significant differences in thalianol levels were observed in mock conditions in the *coi1-16* mutant versus the wt (Fig. 1b). Together, these data support the control of root triterpene biosynthesis by COI1-dependent JA signalling.

To further map the spatiotemporal regulation of the marneral and thalianol BGCs, we profiled the transcriptional changes in root tips treated for 2 h with mock or 50 µM JA at single-cell resolution (Fig. 1c and Supplementary Figs. 2 and 3). Although JA induced marked transcriptional changes in most sampled cells, the uniform manifold approximation and projection (UMAP) representations of mock and JA transcriptomes suggest a differential responsiveness of different cell types to JA (Fig. 1c and Supplementary Figs. 3 and 4). Analysis of Euclidean distances between transcript profiles of the two treatments indicated that cells belonging to the lateral root cap (LRC) or the metaxylem were more responsive, and others, such as vascular initial or pericycle cells, had a reduced responsiveness to JA treatment (Supplementary Fig. 4). Genes in the thalianol BGC showed strong expression upon JA treatment in cells of the root cap, epidermis, cortex, columella, atrichoblast and trichoblast (Fig. 1d and Extended Data Fig. 1). We corroborated these results using a promoter reporter line expressing nuclear localization signal fused to green fluorescent protein (NLS-GFP) under the control of the *THAS* promoter[15], which largely recapitulated the predicted single-cell RNA sequencing (scRNAseq) expression pattern for the *THAS* gene, with low expression in mock conditions and a strong NLS-GFP signal after JA treatment in the root cap and epidermis (Fig. 1e). The genes in the marneral BGC showed similar expression patterns compared to those in the thalianol BGC, with a strong expression pattern upon JA treatment located at the LRC, epidermis and atrichoblast (Fig. 1d and Extended Data Fig. 2). A *ProMRO:GFP-GUS* reporter line confirmed this predicted scRNAseq expression pattern (Fig. 1e). Overall, these results indicate that thalianol and marneral BGCs are specifically expressed in the outer cell layers of the root tips, and their expression is strongly activated by JA.

MYC TFs regulate the expression of triterpene BGCs in root tips

The main regulator of the JA-triggered stress response in Arabidopsis is the clade IIIe basic helix-loop-helix (bHLH) TF MYC2, which is predominantly expressed in roots[20,25,27] and acts redundantly with MYC3 and MYC4 for many JA-dependent responses[20,28]. To assess whether thalianol and marneral BGC expression depends on these TFs, we first analysed BGC transcript accumulation by quantitative reverse transcription PCR (RT-qPCR) in the single *myc2* and the triple *myc2 myc3 myc4* (*mycT*) mutants (Fig. 2a). No differences in transcript accumulation between wt and *myc* mutant lines could be observed for any of the BGC genes in mock conditions. However, after 6 h of JA treatment, JA-induced expression of most genes in the thalianol and marneral BGCs was significantly reduced in roots of the *myc2* and *mycT* mutants compared with the wt (Fig. 2a). Thalianol metabolite profiling of *myc2* and *mycT* roots indicated that although *myc2* roots showed a decrease in JA-induced thalianol levels as compared with the wt (Fig. 1b), the difference was not significant yet. In contrast, the thalianol content

Fig. 1 | Single-cell transcript patterns of genes in the triterpene BGCs in root meristem cells upon JA treatment. a, RT-qPCR showing steady-state transcript levels of genes in the marneral and thalianol BGCs in roots of Col-0 (wt) and *coi1-1* seedlings after a 6 h mock or 50 µM JA treatment. Values on the *Y* axis represent fold-induction compared to mock-treated wt (set to 1). Error bars designate s.e.m. ($n = 3$ biologically independent samples). Statistical significance of differences between genotypes and treatments was determined using two-sided Student's *t*-test (*$P < 0.05$, **$P < 0.005$, ***$P < 0.0005$). **b**, Thalianol metabolite levels in wt, *coi1-16, aos, myc2, mycT, bHLHIVq-1* and *mycT;bHLHIVq-1* seedlings after a 24 h mock or 50 µM JA treatment. Values on the *X* axis represent fold-induction compared to mock-treated wt (set to 1). Error bars designate s.e.m. ($n = 5$ biologically independent samples). Statistical significance of differences between genotypes and treatments was determined using two-sided Student's *t*-test (*$P < 0.05$, **$P < 0.005$, ***$P < 0.0005$). **c**, UMAP representation of the mock- and JA-treated scRNAseq datasets (2 h mock or 50 µM JA treatment). Cell identities are shown by clusters of different colours. **d**, Violin plots showing cell-specific expression of *THAS* and *MRO* upon 2 h mock and 50 µM JA treatment of wt root tips. **e**, Expression profiles of *ProTHAS:NLS-GFP-GUS* and *ProMRO:GFP-GUS* in wt root tips grown on mock or 50 µM JA for 24 h. Scale bars, 20 µm.

https://doi.org/10.1038/s41477-023-01419-8

was significantly reduced compared with the wt after JA treatment of the *mycT* mutants (Fig. 1b). In accordance with the transcript data (Fig. 2a) and as observed for the *coi1-16* mutant, no significant differences in thalianol levels were observed in the *myc* mutants in mock conditions. Given that thalianol and marneral BGC expression was found to be confined to the outer cell layers of the root tips (Fig. 1d,e), we next evaluated the expression patterns of *MYC2*, *MYC3* and *MYC4* in our scRNAseq dataset. Surprisingly, *MYC2* was predicted to show

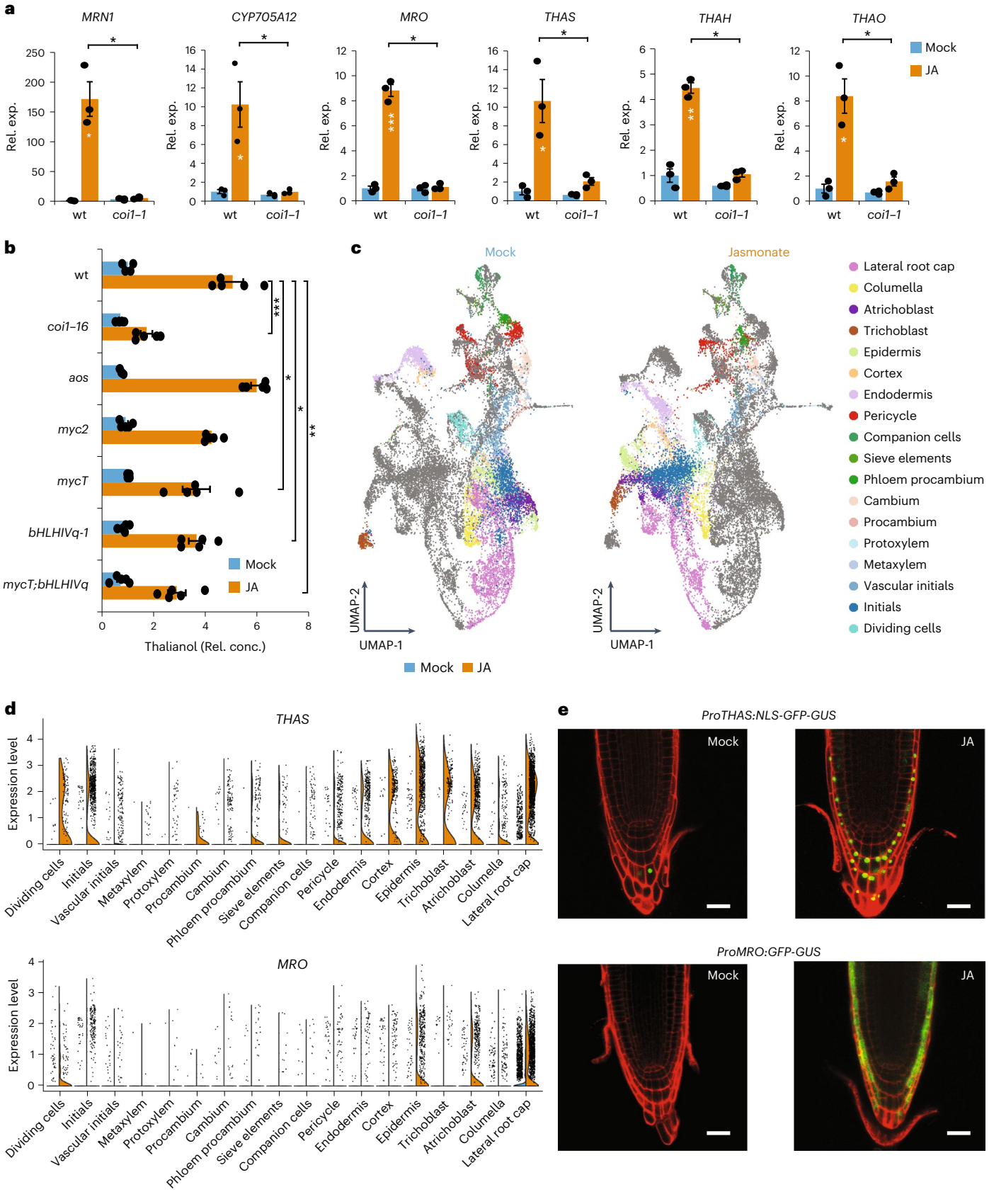

https://doi.org/10.1038/s41477-023-01419-8

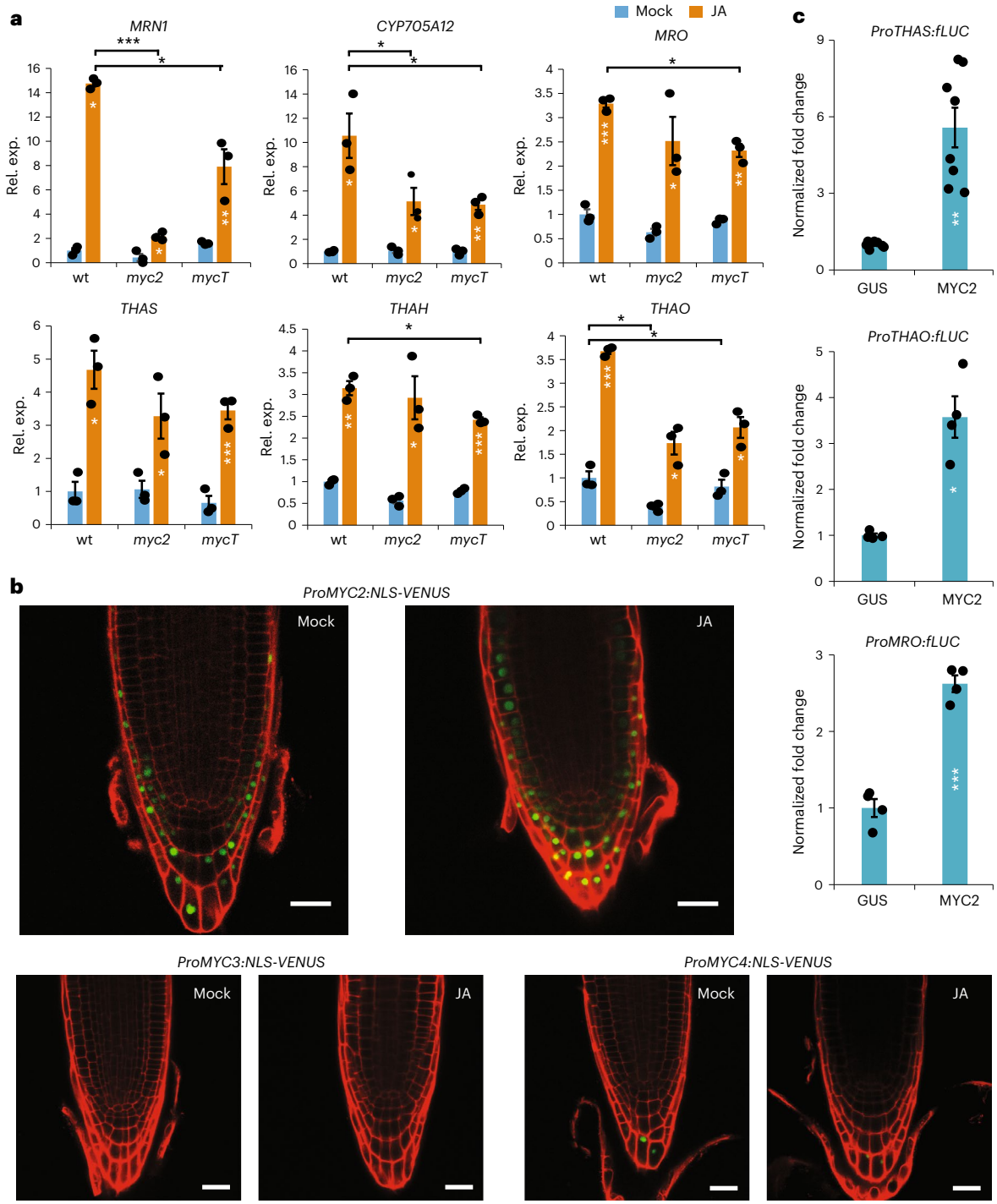

Fig. 2 | Triterpene BGC gene expression depends partially on MYC2. **a**, RT-qPCR showing steady-state transcript levels of genes in the marneral and thalianol BGCs in roots of Col-0 (wt), single *myc2* and triple *myc2 myc3 myc4* (*mycT*) seedlings after a 6 h mock or 50 µM JA treatment. Values on the *Y* axis represent fold-induction compared to mock-treated wt (set to 1). Error bars designate s.e.m. ($n = 3$ biologically independent samples). Statistical significance of differences between genotypes and treatments was determined using two-sided Student's *t*-test (*$P < 0.05$, **$P < 0.005$, ***$P < 0.0005$). **b**, Expression profiles of *ProMYC2:NLS-VENUS*, *ProMYC3:NLS-VENUS* and *ProMYC4:NLS-VENUS* in wt root tips grown on mock or 50 µM JA for 24 h. Scale bars, 20 µm. **c**, Transactivation in transfected *Nicotiana tabacum* protoplasts of the *ProTHAS*-, *ProTHAO*- and *ProMRO*-driven *fLUC* reporters by MYC2. Values on the *Y* axis are normalized fold changes relative to protoplasts cotransfected with the reporter constructs and a *pCaMV35S:GUS* (GUS) control plasmid (set to 1). Error bars designate s.e.m. ($n = 8$ biologically independent samples for *proTHAS*, $n = 4$ biologically independent samples for *ProTHAO* and *ProMRO*). Statistical significance of differences was determined using two-sided Student's *t*-test (*$P < 0.05$, **$P < 0.005$, ***$P < 0.0005$).

a strong and ubiquitous expression in the scRNAseq dataset, independent of JA treatment (Extended Data Fig. 3a). As we expected *MYC2* expression levels to be modified by stresses such as protoplast generation, we next analysed *MYC2* transcript levels in bulk RNA extracted from intact roots or root protoplasts. This demonstrated that protoplast generation strongly increased the accumulation of *MYC2* transcripts as also already reported previously[29], even overruling the JA effect on *MYC2* levels in intact roots (Extended Data Fig. 3b). Notably, this

https://doi.org/10.1038/s41477-023-01419-8

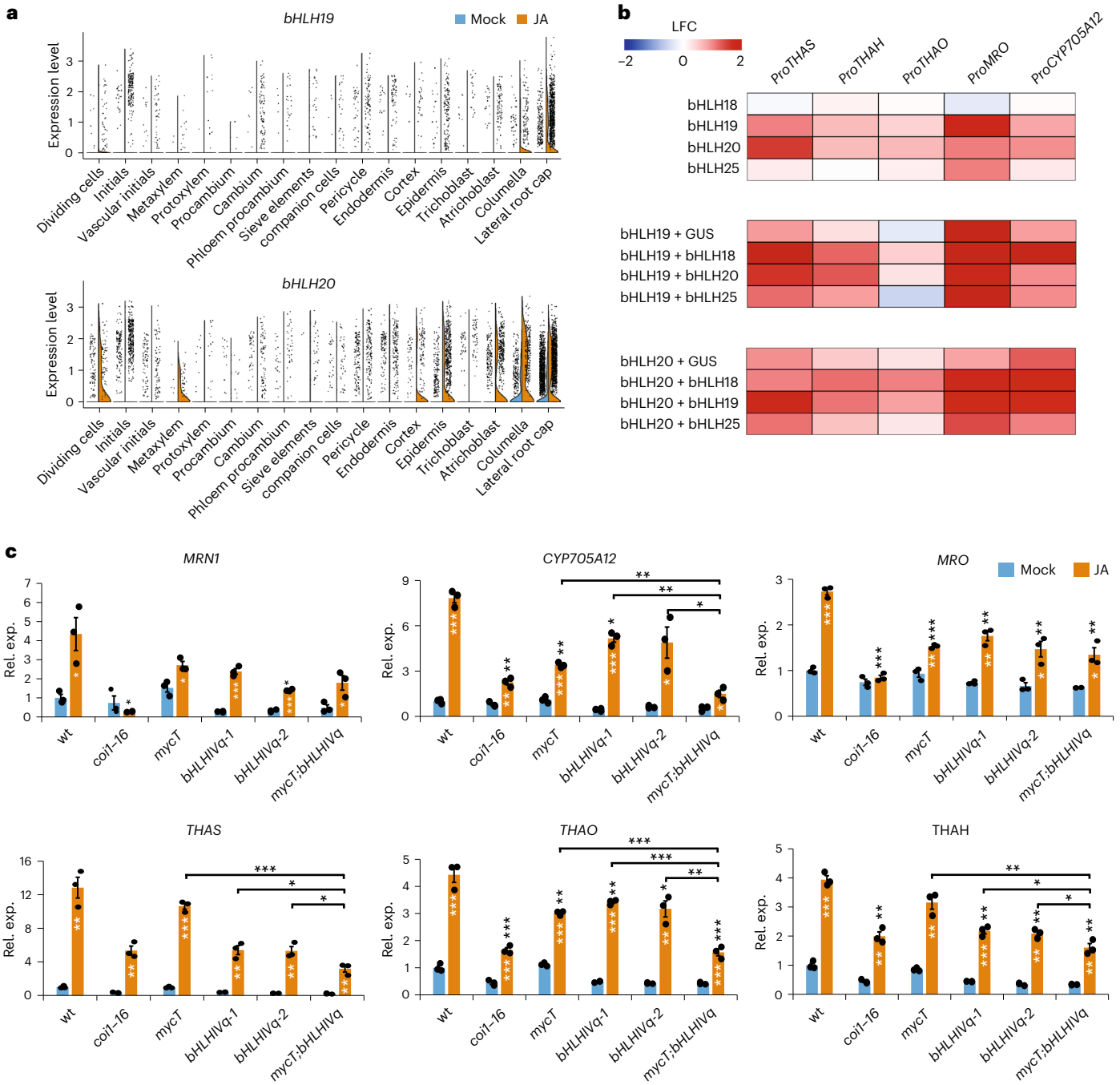

Fig. 3 | Cell-specific activation of genes in the triterpene BGCs is codetermined by MYC2 and bHLH clade IVa TFs. a, Violin plots showing cell-specific expression of *bHLH19* and *bHLH20* in 2 h mock- and JA-treated wt root tips. **b**, Heat maps representing transactivation assays of triterpene BGC *fLUC* reporters (indicated on top) by individual clade IVa bHLH TFs, as well as possible combinations of bHLH19 or bHLH20 with the other clade IVa bHLH TFs. Values are represented as log fold change (LFC) relative to protoplasts cotransfected with the reporter constructs and a *pCaMV35S:GUS* control plasmid. **c**, RT-qPCR showing transcript levels of the marneral and thalianol BGCs in root tips of Col-0 (wt), *coi1-16*, *mycT*, *bHLHIVq-1*, *bHLHIVq-2* and *mycT;bHLHIVq* seedlings after a 6 h mock or 50 µM JA treatment. Values on the *Y* axis represent fold-induction compared to mock-treated wt (set to 1). Error bars designate s.e.m. ($n = 3$ biologically independent samples). Statistical significance of differences between genotypes and treatments was determined using two-sided Student's *t*-test (*$P < 0.05$, **$P < 0.005$; ***$P < 0.0005$).

effect was not observed for *MYC3* or *MYC4*, or any of the genes from the thalianol and marneral BGCs (Extended Data Fig. 3b). As such, expression of *MYC2* cannot be reliably predicted by the scRNAseq data. To overcome this limitation, we used reporter constructs that express *NLS-VENUS* driven by the corresponding *MYC* gene promoters[25]. The expression of *ProMYC2:NLS-VENUS*, but not that of *ProMYC3:NLS-VENUS* or *ProMYC4:NLS-VENUS*, correlated with that of the triterpene BGCs at the epidermis, cortex, LRC and columella (Fig. 2b). Notably, although JA treatment increased the expression of the *ProMYC2:NLS-VENUS* construct, it did not alter the spatial expression pattern (Fig. 2b). Chromatin immunoprecipitation followed by sequencing (ChIPseq) has shown that both thalianol and marneral BGC promoters could be physically bound by MYC2 and MYC3[30]. To verify whether MYC2 can transactivate these genes, we made *fLUC* reporter constructs driven by 2 kb promoter

fragments of the *THAS* (*ProTHAS*), *THAO* (*ProTHAO*) and *MRO* (*ProMRO*) genes and performed transactivation assays in tobacco protoplasts. MYC2 could activate all promoters by at least fivefold compared with the negative control (Fig. 2c), thereby further corroborating its direct role in the JA-mediated activation of triterpene biosynthesis. Taken together, our data support a role for the three MYC TFs in the regulation of triterpene biosynthesis, with MYC2 probably being the most important contributor in this cellular process.

Clade IVa bHLH TFs drive JA induction of triterpene BGCs

While the above-described results demonstrate a role for MYC2 as transcriptional activator for both thalianol and marneral BGCs, the RT-qPCR analyses of the single and triple *myc* mutants suggest the existence of additional factors controlling the JA response. Likewise, the fact that ubiquitous expression of *MYC2* following protoplasting in the scRNAseq data did not coincide with ubiquitous expression of the BGCs suggests the existence of additional factors controlling their spatiotemporal expression (Fig. 1d,e and Extended Data Figs. 1–3). To identify these additional factors, we used our scRNAseq dataset to generate a gene co-expression matrix for *THAS* across all root tip cell types (Extended Data Fig. 4 and Supplementary Table 1). As expected, a list of the 100 most co-expressed genes included the thalianol pathway genes *THAO*, *THAH*, *THAR1*, *THAR2* and *THAA1*, and the marneral pathway genes *MRN*, *MRO* and *CYP75A12*. Furthermore, many known JA-responsive genes were found to be co-expressed, such as JA and glucosinolate biosynthesis genes, confirming the robustness of this dataset. This analysis also identified *bHLH19* and *bHLH20* (*NAI1*), both bHLH clade IVa TFs, which is in agreement with previously reported functions of such clade IVa bHLH TFs in *Catharanthus roseus* and *Medicago truncatula* as regulators of terpene biosynthesis[31,32]. The Arabidopsis bHLH clade IVa also includes *bHLH18* and *bHLH25*, yet the latter two showed overall reduced expression levels in our dataset (Extended Data Fig. 5a). Further predictions of expression by scRNAseq and validation by RT-qPCR indicated that JA induces the expression of these clade IVa TFs in similar cell types as those of the triterpene BGCs, that is, in the epidermis, atrichoblast, cortex, columella and LRC (Fig. 3a and Extended Data Fig. 5a). A reporter line carrying the *ProbHLH19:GFP-GUS* gene confirmed their expression in the outer cell layers of wt root tips, in which *bHLH19* expression was highly JA-induced in the tissues of the stele, LRC, epidermis and cortex and, to a lesser extent, in columella cells (Extended Data Fig. 5b). Moreover, the JA inducibility of *bHLH19* and *bHLH20* was dependent on COI1 (Extended Data Fig. 5c). We then assessed whether JA-induced expression of the clade IVa bHLH genes involves the MYCs. Compared with the wt, JA-induced expression was significantly reduced for all clade IVa genes in the *mycT* line (Extended Data Fig. 6a). The promoter regions of Arabidopsis bHLH clade IVa genes contain a G-box (Supplementary Table 2) and have been shown to be bound by MYC2[30,33]. We accordingly tested whether MYC2 could transactivate these promoters and whether they can be transactivated by themselves. Because *bHLH19* and *bHLH20* showed a strong and significant upregulation upon JA treatment and were predicted to be the most highly expressed in root tips (Fig. 3a and Extended Data Figs. 5 and 6), we cloned 1,926 bp (*ProHLH19*) and 2,000 bp (*ProbHLH20*) promoter fragments and performed transactivation assays using wt MYC2, desensitized MYC2^{D105N}, bHLH19 and bHLH20. The MYC2^{D105N} mutation abolishes the interaction between MYC2 and most JAZ proteins, by which transactivation becomes typically more pronounced[34]. Strong transactivation of both *ProHLH19* and *ProHLH20* was triggered by MYC2^{D105N}, whereas wt MYC2 had a moderate effect (Extended Data Fig. 6b). Conversely, bHLH19 and bHLH20 only had minor transactivation effects on their respective promoters. Taken together, our data indicate that, similar to the genes of the thalianol and marneral BGCs, the expression of the Arabidopsis clade IVa bHLH TF genes is induced by JA in outer root tip cell layers through the canonical signalling module that involves COI1 and MYCs.

To verify whether the bHLH clade IVa TFs could also directly modulate the expression of thalianol and/or marneral biosynthesis genes, we first performed transient promoter transactivation assays in tobacco protoplasts (Fig. 3b and Supplementary Fig. 5). This analysis suggested both redundant and additive activities for these TFs. For instance, when tested alone, bHLH19, bHLH20 and bHLH25 showed similar capacities and preferences for transactivating BGC promoters. Combining bHLH19 with bHLH18, bHLH20 or bHLH25 increased the transactivation of the thalianol BGC promoters compared with bHLH19 alone, reflecting the additive contributions of these TFs in the regulation of the expression of the triterpene BGCs (Fig. 3b). Similarly, combining bHLH20 with either bHLH18 or bHLH19 resulted in an additive transactivation of the marneral promoters. These results support the concerted actions of MYC and bHLH clade IVa TFs to activate the expression of the triterpene BGCs. We next generated mutant lines for the four loci encoding the bHLH clade IVa TFs (Supplementary Fig. 6). These mutations were introduced in both the wt and the *mycT* background, resulting in two independent quadruple mutant lines hereafter named *bHLHIVq-1* and *bHLHIVq-2*, and a septuple mutant line named *mycT;bHLHIVq*. We inquired whether the expression of genes in the triterpene BGCs was compromised in these lines after JA induction. Transcript levels of all triterpene genes were already reduced in the absence of JA in the *bHLHIVq* lines compared with the wt (Fig. 3c). Furthermore, the *bHLHIVq* lines showed an overall significantly reduced JA induction of both marneral and thalianol BGCs that was more pronounced than in the *mycT* mutant for the thalianol genes, further supporting a major role for the bHLH clade IVa TFs in the regulation of this pathway. Accordingly, the *mycT;bHLHIVq* septuple mutant showed even less JA induction for most tested genes in the triterpene BGCs compared with either the *bHLHIVq* or the *mycT* lines (Fig. 3c). Remarkably, in most cases, such as for *CYP705A12, THAS, THAO* and *THAH*, the JA induction of triterpene gene expression in the *mycT;bHLHIVq* mutant was attenuated to levels comparable to those in the *coi1-16* mutant, which is a weak *coi1* allele. In accordance with the transcript data, also the thalianol content of the *bHLHIVq* mutant was significantly reduced compared with the wt (Fig. 1b). The *mycT;bHLHIVq* mutants showed an additional reduction (although not significant) compared with the *mycT* or *bHLHIVq* mutants after JA treatment. Together, these data confirm the redundant roles of bHLH clade IVa and MYC TFs in the regulation of triterpene biosynthesis in Arabidopsis roots.

Fig. 4 | Expression of triterpene genes in the BGCs is coactivated by GL2 and repressed in inner root tissues by the DOF factor DAG1. a, Motif mapping-based network of triterpene biosynthesis genes and their predicted TF regulators. Red: HDG-type TFs; magenta: DOF-type TFs; grey: other TFs; green: Thalianol BGC; yellow: Marneral BGC; cyan: MYC-type TFs; blue: bHLH-type TFs. **b**, Violin plot showing the tissue-specific expression profile of *DAG1* and *GL2* in mock- and JA-treated conditions. **c**, Histochemical analysis of the spatial expression of *ProDAG1:GUS* in mock- and JA-treated conditions. Scale bars, 20 µm. Roots from at least 3 seedlings were analysed with similar results. **d**, Heat map representing transactivation assays of triterpene BGC promoters driving *fLUC* reporters (indicated on top) by individual and combinations of clade IVa bHLH TFs, MYC2^{D105N}, DAG1 and GL2. Values are represented as LFC relative to protoplasts cotransfected with the reporter constructs and a *pCaMV35S:GUS* control plasmid. **e**, RT-qPCR showing transcript accumulation levels of the indicated genes in the marneral and thalianol BGCs in roots of Ws-4 wt, *dag1* and *35S:DAG1-HA;dag1* (*DAG1-OE*) seedlings after a 2 h mock or JA treatment. **f**, RT-qPCR showing transcript accumulation levels of the indicated genes in the marneral and thalianol BGCs in roots of Col-0 wt, *gl2-5* and *gl2-3* seedlings after a 2 h mock or JA treatment. Values on the *Y* axis represent fold-induction compared to mock-treated wt (set to 1). Error bars designate s.e.m. ($n = 3$ biologically independent samples). Statistical significance of differences between genotypes and treatments was determined using two-sided Student's *t*-test (*$P < 0.05$, **$P < 0.005$, ***$P < 0.0005$).

https://doi.org/10.1038/s41477-023-01419-8

Redundant coactivators/repressors set triterpene BGC cell specificity

Although the transcription of the genes encoding the bHLH clade IVa TFs and of the triterpene BGCs is activated by MYC2, these genes maintain cell-specific expression patterns in our scRNAseq datasets (Fig. 1d,e and Extended Data Figs. 1 and 2), contrary to MYC2 (Extended Data Fig. 3a). Hence, we questioned whether additional regulatory components may confine spatial expression of these genes and overrule JA or other elicitor effects such as protoplast generation (Extended Data Fig. 3b). Triterpene BGCs have been shown to be located at transcriptionally active chromosomal sites in root tissues[13]. We therefore postulated that cell-specific expression of the triterpene BGCs is controlled either by (1) 'repressive' TFs that are constitutively and specifically expressed in inner root tip tissues to thereby suppress the expression of triterpene

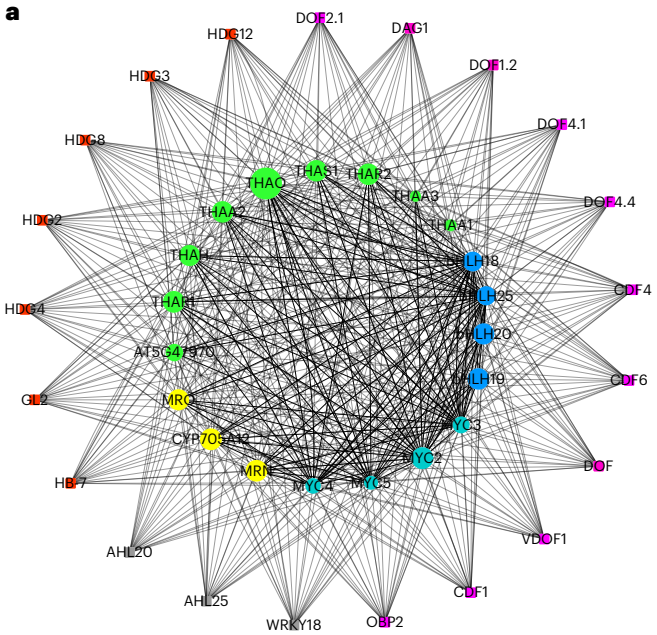

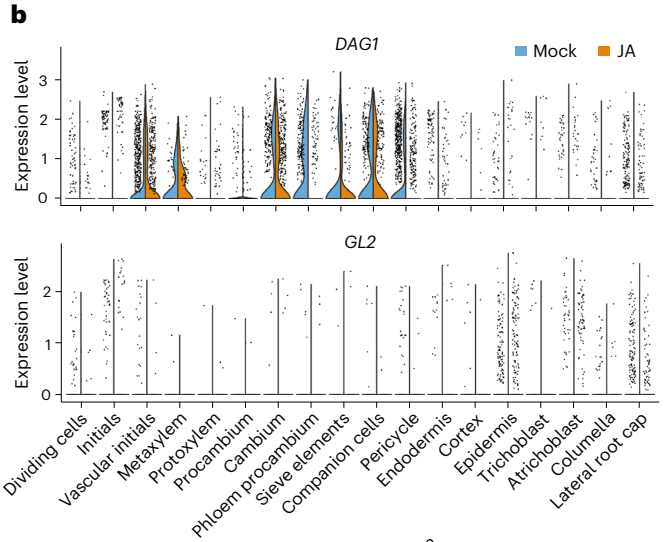

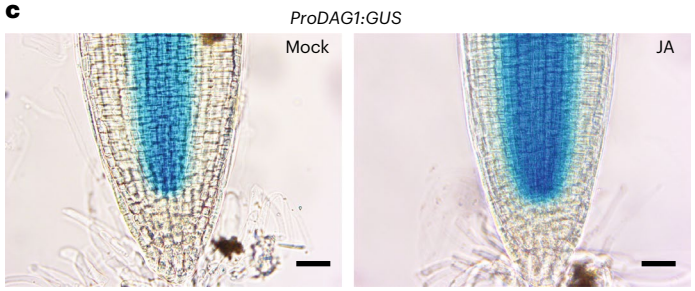

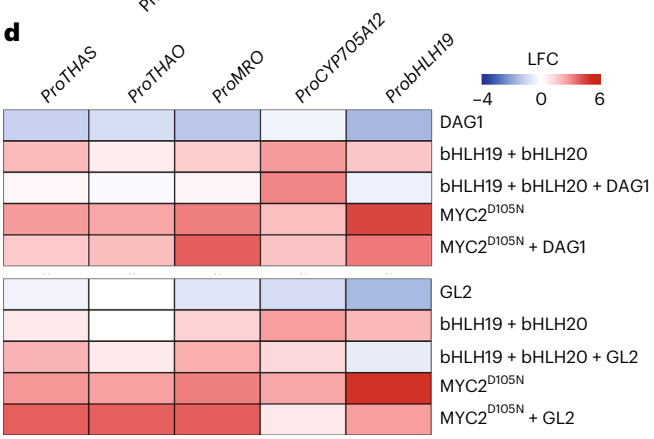

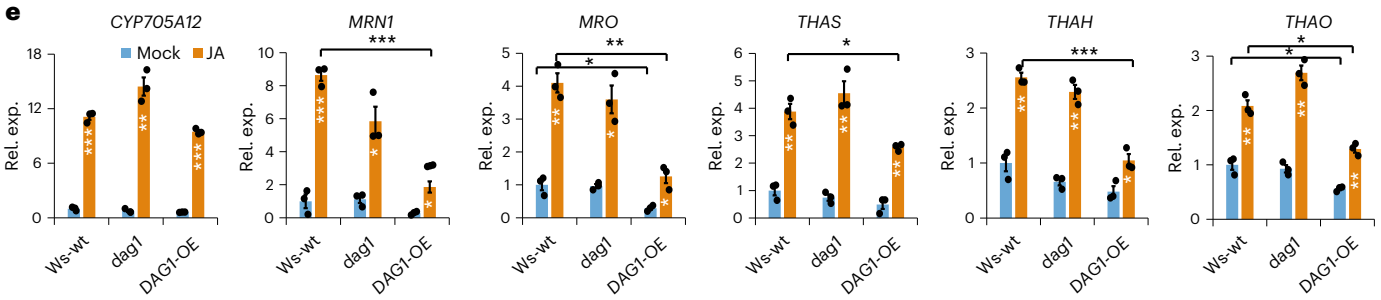

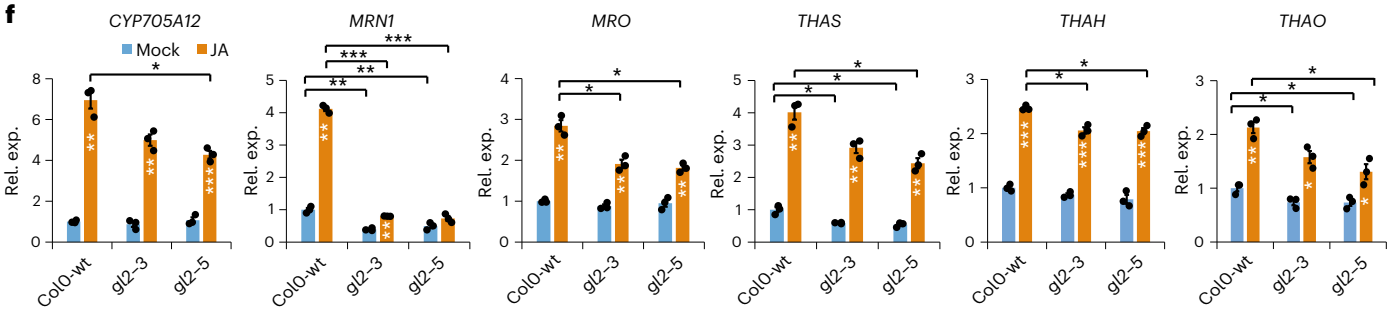

biosynthesis genes, or (2) additional 'activating' factors that are specifically expressed in outer root tip tissues and whose presence is essential to coactivate the transcription of triterpene pathway genes. We searched for such TFs using a motif collection that consists of 1,699 position weight matrices representing the DNA-binding sites for 1,143 Arabidopsis TFs. We accordingly mapped TFs potentially binding to every gene in the thalianol and marneral BGCs, as well as those encoding the MYC and bHLH clade IVa TFs. This analysis identified a set of 21 TFs, of which 11 belonged to the DNA-binding one finger (DOF) family and 7 to the homeodomain glabrous (HDG) family (Fig. 4a and Supplementary Table 3). Most of the DOF-type TFs were predicted to be expressed in the inner root tip cell layers, whereas HDG-type TFs were rather predicted to be expressed in outer root tip cell layers (Extended Data Fig. 7). Markedly, expression of all these DOF- and HDG-type TFs was predicted to be insensitive to JA treatment in the outer root tip cell layers, which was further confirmed by analysis of root tips of a mock- and JA-treated *ProDAG1:GUS* reporter line (Fig. 4b,c and Extended Data Fig. 7).

Members of the HDG family have been shown to be involved in root terpene biosynthesis and epidermis development[35]. For this reason, we selected GL2, HDG2 and HDG5 for further characterization and performed transient promoter transactivation assays in tobacco protoplasts. Transfection with either GL2, HDG2 or HDG5 alone did not markedly affect the activity of the *ProTHAS* reporter (Extended Data Fig. 8). However, cotransfection of GL2 with either $MYC2^{D105N}$ or bHLH19 and bHLH20 had a pronounced synergistic effect on BGC reporter activities (Fig. 4d, Extended Data Fig. 8 and Supplementary Fig. 7b). The effect of the other HDGs was less pronounced or consistent; nonetheless additive trends could be observed in some combinations (Extended Data Fig. 8). Overall, this supports a redundant role for these HDG TFs as coactivators of the root triterpene BGCs. We next carried out a RT-qPCR-based expression analysis in two available *gl2* mutant alleles[36,37]. The effects of loss-of-GL2-function in the two examined alleles resulted in a consistent decrease in both the basal expression and JA induction of genes in the root triterpene BGCs, being most pronounced for the marneral BGC (Fig. 4e).

For the DOF-type TFs, we selected DAG1 and vDOF1 (DOF4.6), given their reported opposed expression patterns compared with genes in the triterpene BGCs (Fig. 4b and Extended Data Fig. 7)[38,39] and their transcriptional repressor activities[39,40]. DAG1, but not vDOF1, showed strong repression activities on promoters in both the thalianol and marneral BGCs, as well as on *ProbHLH19* in protoplast assays (Fig. 4d, Extended Data Fig. 9 and Supplementary Fig. 7a). Furthermore, cotransfection of DAG1 with either $MYC2^{D105N}$ or bHLH19 and bHLH20 counteracted the transactivation capacities of the transcriptional activators (Fig. 4d and Supplementary Fig. 7a). These results support a role for DAG1 as a cell-specific repressor of triterpene pathway genes. Hence, we subsequently analysed whether the available *dag1* mutant or *ProCaMV35S:DAG1* (*DAG1-OE*) lines[41,42] show altered triterpene gene expression. Expression of *DAG1* by the *ProCaMV35S* promoter, which drives ectopic expression in the outer root cell layers (Supplementary Fig. 8), indeed resulted in a significantly decreased expression of most genes in the triterpene BGCs under JA treatment as compared with wt plants (Fig. 4e), corroborating an in planta function for this TF as a triterpene BGC repressor. However, no significant differences were observed between the *dag1* and wt lines, either in mock or JA conditions, probably pointing to redundant functions with yet undetermined additional repressors, plausibly other DOF TFs, to confine the expression of triterpene biosynthesis to specific root cells.

Discussion

Together with the vast variety in structures and bioactivities of specialized metabolites, complex regulatory networks coevolved to ensure correct expression of the corresponding biosynthetic pathways. Whereas regulators involved in the stress-mediated induction of specialized metabolism have been identified repeatedly, knowledge of the regulators driving cell specificity of specialized metabolite pathways is scarce. Here, via scRNAseq analysis, we identified a transcriptional regulatory network that underlies both the cell-specific and stress-inducible expression of Arabidopsis triterpene biosynthesis in the root tip (Extended Data Fig. 10). Expression of the genes in the thalianol and marneral BGCs is enhanced by JA via the canonical signalling cascade and limited to the outer layers of root tip tissues. The latter is consistent with the function played by these triterpenes in microbiome recruitment and modulation of root growth[7,15]. Previous work has shown that the spatial expression of the thalianol and marneral BGCs differs in the leaves and roots, where these clusters are silenced and transcriptionally active, respectively[13]. Here we provide evidence for the mechanism of transcriptional regulation of these BGCs in root tips, through a complex interplay between cell-specific activator and repressor TFs. A redundant set of bHLH-type TFs from two distinct clades, assisted by HDG-type coactivator TFs, promotes triterpene biosynthesis in the outer cell layers. Interestingly, the expression of the genes in the thalianol and marneral BGCs is rescued in the *jazQmycT* mutant line, suggesting that, in addition to the MYC TFs, other yet unidentified JAZ-interacting TFs may activate the expression of the triterpene BGCs and/or bHLH clade IVa TFs[26]. This is also corroborated by the thalianol transcript and metabolite profiling of the *mycT*, *bHLHIVq* and *mycT;bHLHIVq* mutant roots in this study, in which the final reduction in thalianol accumulation after JA treatment is not as drastic as that in the *coi1-16* line, suggesting that other as yet unidentified COI1-dependent TFs may contribute to the activation of triterpene biosynthesis genes. Therefore, the model of the regulatory network that we propose here does not reflect the full complexity yet (Extended Data Fig. 10). Conversely, other regulatory TFs, hallmarked by the DOF-type TF DAG1, prevent the expression of the triterpene pathway genes in inner root tip tissues. Notably, in its function as a repressor, DAG1 is capable of overruling the activity of MYC2 and the other bHLH TFs in root tips. The observed redundancy within this model implicates the emergence of a very robust regulatory network, wherein both cell-specific activation and repression are subjected to strong selective pressure to ensure that bioactive metabolites are produced at the right place at the right time to promote survival and interaction with the environment, and avoid self-toxicity or unnecessary metabolic investments. This regulatory network may also involve so-called super enhancers (SEs), a cluster of *cis*-regulatory elements that can increase the transcription of their cognate genes. Very recently, such an SE has been identified within the thalianol BGC, and its deletion resulted in the transcriptional repression of genes in the thalianol BGC[43]. How specific such SEs may work in terms of target genes and/or hormone-responsive and/or cell-specific expression remains to be determined. We postulate that analogous regulatory frameworks are applicable to many other cell-specific plant specialized metabolite pathways in Arabidopsis and beyond, and during evolution-involved recruitment of identical, similar and/or distinct sets of redundant activators and repressors.

Methods

Plant material and treatments

The *coi1-1*, *coi1-16*, *myc2 (jin1-2)* and *myc2 myc3 myc4* mutants, and the *ProTHAS:NLS-GFP-GUS*, *ProMYC2:NLS-VENUS*, *ProMYC3:NLS-VENUS* and *ProMYC4:NLS-VENUS* reporter lines are in the *A. thaliana* Col-0 background and were previously described[20,25,27,44–46]. The *dag1*, *dag1 DAG1*-OE and *ProDAG1-GUS* lines are in the Wassilewskija (Ws) background and were also previously described[38,41]. The *ProMRO:GFP-GUS* and *ProbHLH19:GFP-GUS* lines were generated by floral dip of *A. thaliana* in the Col-0 ecotype using *Agrobacterium tumefaciens* strain C58C1. Knockout mutants of the *bHLH IVa* genes were generated in the Col-0 and *mycT* backgrounds using CRISPR-Cas9 genome editing technology. Single guide RNAs (sgRNAs) targeting the first or second exons of *bHLH18*, *bHLH19*, *bHLH20* and *bHLH25* were designed

by CRISP-OR (http://crispor.tefor.net/)[47]. For each target gene, two specific sgRNAs were selected and synthesized as indicated in Supplementary Fig. 6, using the primers listed in Supplementary Table 4. A single CRISPR/Cas9 vector containing the *Cas9* gene and eight sgRNAs targeting all four *bHLH IVa* genes simultaneously was generated using GreenGate technology as previously described[48]. Briefly, for a pair of two gRNA target sites, two oligonucleotides with 16 bp overhangs were ordered (primers P25-P32; Supplementary Table 4). The primers were annealed on the template pEN-2x*AtU6*, then *BbsI*-ligated into the Golden Gate entry vectors pGG-A-*AtU6ccdB*-B, pGG-B-*AtU6ccdB*-C, pGG-C-*AtU6ccdB*-D or pGG-D-*AtU6ccdB*-E. Four Golden Gate entry modules, each containing two sgRNAs, were assembled into the binary vector pFASTGK-*AtCas9*-A-*ccdB*-G. CRISPR constructs were transfected into *A. tumefaciens* C58C1 (pMP90) and used to transform Arabidopsis Col-0 and *mycT* using floral dip. Primary transformants (T1) were selected on kanamycin (50 μg ml^{-1}) and the genomic region spanning the predicted Cas9 cut site was sequenced using primers P35-P42 (Supplementary Table 4). T2 plants were monitored for segregation of the T-DNA locus using kanamycin resistance and were genotyped using Cas9-specific primers (P33/34; Supplementary Table 4) to identify null segregants. In these plants, all four bHLH loci were reanalysed using PCR to identify genotypes that were now non-chimaeric and either homo- or hetero-allelic. The most promising plants were then propagated to T3, in which the absence of Cas9 and the homogeneous state of the edited allele were confirmed by PCR and sequencing. The Arabidopsis Genome Initiative identifiers for the genes used in this study are listed in Supplementary Table 5.

Arabidopsis seeds were surface-sterilized for 5 min in 70% ethanol to which 1% Tween-20 was added, followed by a 5 min incubation in 95% ethanol. Seeds were dried for 3 h before plating. For treatments, seeds were placed on nylon meshes (Sefar, 03-20/14) on 0.5x Murashige and Skoog (MS) medium (including vitamins), 0.5% MES (pH 5.8) and 0.7% phytoagar plates. After stratification for 2 d at 4 °C, the plates were transferred to standard growth conditions (21 °C, 16 h/8 h light/dark regime) and grown vertically for 8 d. For transcript analyses, the meshes with seedlings were then transferred to plates containing 50 μM JA in ethanol (Sigma-Aldrich) or mock (ethanol) and roots were collected 6 h after treatment. For confocal imaging and *β*-glucuronidase (GUS) histochemical analyses, seedlings were transferred to plates containing 50 μM JA in ethanol or mock for 24 h. For comparative expression analysis in Col-0 and the *coi1-1* mutant, seedlings were first grown for 5 d on mock plates or plates containing 50 μM JA, respectively, to enable selection of homozygous *coi1-1* plants, and subsequently transferred to plates with ½ MS (including vitamins), 0.5% MES (pH 5.8) and 1% phytoagar without JA and grown vertically on a nylon mesh for 7 d. Before sampling the roots, the mesh was transferred to plates containing 50 μM JA or mock for 6 h. For metabolite analyses, 5-day-old seedlings were transferred on 6-well culture plates containing liquid ½ MS (including vitamins), 0.5% MES (pH 5.8) and 1% sucrose, and grown in standard light/dark growth conditions with shaking (90 r.p.m.) for 8 d as previously described[15]. For treatment, the medium was replaced with fresh liquid medium containing 50 μM JA in ethanol or mock, then roots were collected 24 h after treatment, flash-frozen and freeze-dried.

Subcellular protein localization

Fluorescence (GFP or Venus) was monitored in primary root cell tips of 5-day-old seedlings grown vertically on ½ MS agar medium. Before imaging, root tips were stained with propidium iodide and mounted on slides. Fluorescence was followed with a Zeiss LSM 710 confocal microscope using ×40 magnification. Images were then processed using Zeiss Zen 2 and ImageJ (v.1.53c) softwares. All optical cross sections were made in the middle of the meristem, determined by the quiescent centre on one end and the first elongating cortex cell on the other end.

GUS histochemical analysis

Histochemical GUS staining was performed in 5-day-old seedlings grown vertically on ½ MS agar medium. The plant material was incubated at 37 °C in the dark for 2 h in a staining buffer containing 1 mM 5-bromo-4-chloro-3-indolyl*ß*-D-glucopyranoside sodium salt (X-Gluc), 0.5% Triton X-100, 1 mM ethylenediaminotetraacetic acid (EDTA, pH 8.0), 0.5 mM potassium ferricyanide ($K_3Fe(CN)_6$), 0.5 mM potassium ferrocyanide ($K_4Fe(CN)_6$) and 500 mM sodium phosphate buffer (pH 7.0). The reaction was terminated by replacing the staining buffer with 70% ethanol. The material was mounted in 25% lactic acid:50% glycerol and analysed with an Olympus BX51 microscope equipped with a Hitachi DK-H32 camera.

Promoter transactivation assays in tobacco protoplasts

For transactivation assays, the promoters of *bHLH19* (*ProHLH19*) and *bHLH20* (*ProbHLH20*) were isolated using primer pairs P1/2 and P3/4 (Supplementary Table 4), respectively, and cloned into pGG-AB before transferring to pGGIB-U1U2 using Golden Gate cloning technology (New England Biolabs). Promoters of *THAS* (*ProTHAS*), *THAH* (*ProTHAH*), *THAO* (*ProTHAO*), *MRO* (*ProMRO*) and *CYP705A12* (*ProCYP705A12*) were isolated using primer pairs P5/6, P7/8, P9/10, P11/12 and P13/P14 (Supplementary Table 4), respectively, and BP-recombined into pDONR221 (Invitrogen). The coding sequences (CDSs) of *bHLH18*, *bHLH19*, *bHLH20* and *bHLH25* were isolated using primers P15/16, P17/18, P19/20 and P21/22 (Supplementary Table 4), respectively, and cloned into pDONR207 (Invitrogen). The entry plasmids were sequence-verified and subsequently LR-recombined into pGWL7 for the promoters and p2GW7 for the CDSs using Gateway technology (Invitrogen). The CDSs of *DAG1*, vDOF1, GL2, HDG2 and HDG5 were isolated using primers P23/24, P69/70, P71/72, P73/74 and P75/76 (Supplementary Table 4), respectively, and cloned into pGG-CD before transferring to pGGIB-U1U2. We cloned MYC2 in MYC2^{D105N} and p2GW7 as previously described[34].

Transient promoter transactivation assays in tobacco protoplasts were performed essentially as previously described[49]. In all cases, a *ProCaMV35S*-driven intron-containing *GUS* construct was used as control transformation. Normalization of firefly luciferase activity was achieved using a *ProCaMV35S*-driven *Renilla* luciferase cotransfection. Measurements were performed with the GloMax Navigator microplate luminometer and the dual-luciferase reporter assay system (Promega).

RNA extraction and qRT-PCR analysis

Total RNA was isolated from roots using the RNeasy plant mini kit (Qiagen) and 1 μg was used for complementary DNA synthesis using the qScript cDNA SuperMix kit (Quanta-Bio). Quantitative RT-PCR (RT-qPCR) was performed as previously described[32] using primers P43-P64 (Supplementary Table 4). RT-qPCR was done with a Lightcycler 480 (Roche) with SYBR Green QPCR master mix (Stratagene). Reactions were done in triplicate and qBase was used to quantify relative expression. For normalization, housekeeping genes *PROTEIN PHOSPHATASE 2A SUBUNIT A3* (*PP2A; At1g13320*, primer pair P65/66) and *MONENSIN SENSITIVITY1* (*MON1; AT2G28390*, primer pair P67/68) were used.

scRNAseq

Single-cell RNA sequencing was performed as previously described[50] with the following modifications.

Protoplasting conditions and FACS

Six-day-old seedlings were transferred to 50 μM JA-supplemented medium or an equal volume of DMSO as mock treatment and allowed to grow for 2 h. Note that the DMSO mock sample was identical to the one described in ref. 51, as these experiments were performed together. The root tips were then cut and incubated in protoplasting solution B (1.5% (w/v) cellulysin and 0.1% (w/v) pectolyase in solution A (600 mM mannitol, 2 mM $MgCl_2$, 0.1% (w/v) bovine serum albumin, 2 mM $CaCl_2$,

2 mM MES, 10 mM KCl pH 5.5)) for approximately 1 h at room temperature. Cells were filtered through a 70 µm cell strainer and spun down at 200 *g* for 6 min, resuspended in solution A, filtered through a 40 µm cell strainer and stained for live/dead using 4′,6-diamidino-2-phenylindole (DAPI) at a 14 µM final concentration. Cells were sorted on a BD Aria II cell sorter and protoplasts without the DAPI signal were selected for further analysis.

10X Genomics sample preparation, library construction and sequencing

Sorted cells were centrifuged at 400 *g* at 4 °C and resuspended in solution A to yield an estimated concentration of 1,000 cells per µl. Cellular suspensions were loaded on a Chromium Single Cell 3′ GEM, Library and Gel Bead kit (V3 chemistry, 10X Genomics) according to manufacturer instructions. Sequencing libraries were loaded on an Illumina HiSeq4000 sequencing system and sequenced following recommendations of 10X Genomics at the VIB Nucleomics Core (VIB).

Raw data processing and generation of gene expression matrix

Demultiplexing of the raw sequencing data was done by the 10x CellRanger v.3.1.0 software 'cellranger mkfastq', which wraps Illumina's bcl2fastq. The fastq files obtained after demultiplexing were used as input for 'cellranger count', which aligns the reads to the *A. thaliana* reference genome (EnsembleTAIR10.40) using STAR and collapses them to unique molecular identifier (UMI) counts. The result is a large digital expression matrix, with cell barcodes as rows and gene identities as columns. Initial filtering in CellRanger recovered 11,569 cells for the mock-treated and 9,660 cells for the JA-treated sample. To ensure that we only used high-quality cells for further analysis, we used the filtered data provided by cell ranger. This corresponds to 26,756 mean reads per cell in the mock-treated sample and 34,275 mean reads per cell in the JA-treated sample.

Data analysis (clustering, identity assignment, differential gene expression, quality control and co-expression)

All analyses were performed in R (v.4.2.0). Preprocessing of the data was done using the scater package (v.1.10.1) according to a previously proposed workflow[52]. Outlier cells were identified on the basis of 2 metrics (library size and number of expressed genes) and were tagged as outliers when they were 4 median absolute deviations away from the median value of these metrics across all cells. Normalizing the raw counts, detecting highly variable genes, finding clusters and creating *t*-distributed stochastic neighbour embedding (t-SNE) plots were done using the Seurat pipeline (v.3.2.3). Differential expression analysis for marker gene identification per subpopulation was based on the non-parametric Wilcoxon rank-sum test implemented within the Seurat pipeline. Clusters with the same cell annotation based on gene expression analysis were combined to generate a more comprehensible dataset. Potential doublets were identified using the DoubletFinder algorithm (v.2.0.0)[53]. The number of high-confidence doublets was below 1% (113 out of 11,313 cells for the mock-treated sample and 96 out of 9,572 cells for the JA-treated sample). For comparing mock to JA treatments, averaged expression levels for each cell type were calculated on the log-normalized UMI counts of the scRNAseq data to build an expression matrix. Pairwise Euclidean distances were calculated between the control and JA-treated versions of the same cell type, as an estimator of the effect of JA treatment on the expression profile of each cell type. Genes co-expressed with the *THAS* gene were identified by computing the Pearson correlation coefficient on the log-normalized UMI counts from the scRNAseq dataset. Genes were next sorted from high to low correlation and the top 100 genes were extracted for further analysis.

TF mapping to promoters of the triterpene BGCs

TF motifs modelled as position weight matrices (PWMs) were retrieved from the CisBP 2.00 (downloaded in December 2019)[54] (http://cisbp.ccbr.utoronto.ca/) and JASPAR2020[55] databases (https://jaspar.genereg.net/) and combined with a collection of manually curated motifs[56]. A total of 1,699 motifs corresponding to 1,143 TFs were collected. TF motifs were mapped to a gene's regulatory regions using Cluster Buster (version compiled in September 2017[57]) and FIMO (v.4.11.3[58]). Cluster Buster was run with the -c parameter set to 0 and PWMs were scaled to 0–100. FIMO was run with default parameters and PWMs were scaled to 0–1. The regulatory regions used for motif mapping were extracted from Arabidopsis Araport11[59], only retaining the longest splicing variants, downloaded from PLAZA Dicots 4.5[60] (https://bioinformatics.psb.ugent.be/plaza/versions/plaza_v4_5_dicots/). These regions were defined as 5,000 bp upstream and 1,000 bp downstream from translation start/stop sites. Introns were included in the regulatory regions, while coding exons were excluded. If another gene was present within the 5,000 bp–1,000 bp window, this region was cut where the other gene started. Finally, mappings from Cluster Buster and FIMO were combined into an ensemble motif mapping gene regulatory network (GRN), following a previously described protocol[61]. Next, the ensemble GRN was queried for TFs that were directly connected to each of the triterpene BGCs and were selected for further analysis.

Thalianol profiling

For thalianol measurements, approximately 100 mg of fresh root material was extracted with 1 ml of methanol. Metabolite extraction was performed for 1 h at room temperature, followed by centrifugation for 10 min at 20,800 *g*. Of the supernatant, 50 µl was collected and evaporated to dryness under vacuum. The remaining plant material was lyophilised for dry weight determination. The residue obtained from metabolite extraction was trimethylsilylated using 50 µl derivatization mixture (*N*-methyl-*N*-(trimethylsilyl)trifluoroacetamide:pyridine in a 5:1 ratio). The derivatized samples were shaken for 1 h at room temperature. Gas chromatography–mass spectrometry (GC–MS) analyses were performed on an Agilent 7250 QTOF-MS equipped with an Agilent 7890B GC system. Derivatized sample (1 µl) was injected in splitless mode with the injector port set to 280 °C. All biological samples were analysed at random and pooled samples were included for system reproducibility. Separation was achieved with a VF-5ms column (40 m × 0.25 mm, 0.25 µm; Varian CP9013; Agilent) with helium carrier gas at a constant flow rate of 1.2 ml min^{-1}. The oven was held at 80 °C for 1 min, ramped to 320 °C at a rate of 10 °C min^{-1} and then held at 320 °C for 5 min. MS transfer line, MS ion source and quadrupole were held at 280 °C, 230 °C and 150 °C, respectively. The MS detector was operated in electron impact mode at 70 eV. Full EI-MS spectra were recorded by scanning the *m*/*z* range of 50–800 with a solvent delay of 6 min. Identification of thalianol was conducted by comparison with the retention time and mass spectrum of a pure standard[7]. Peak areas were integrated using Masshunter Qualitative Analysis software (Agilent) (v.10.0 build 10.0.10305.0) and normalized against the dry weight of the samples.

Reporting summary

Further information on research design is available in the Nature Portfolio Reporting Summary linked to this article.

Data availability

The scRNAseq data are accessible via an online browser tool (http://bioit3.irc.ugent.be/plant-sc-atlas/) and raw data are deposited at NCBI with GEO numbers GSE179820 and GSE212826 for the mock- and JA-treated root tips, respectively. All other data generated for this study are included either in the main paper, Extended Data, or the Supplementary Information. Material requests should be directed to the corresponding author. Published data for TF motif mapping were retrieved from CisBP 2.00 (downloaded in December 2019: http://cisbp.ccbr.utoronto.ca/) and JASPAR2020 (https://jaspar.genereg.net/). The regulatory regions used for motif mapping were downloaded

from PLAZA Dicots 4.5 (https://bioinformatics.psb.ugent.be/plaza/versions/plaza_v4_5_dicots/). Source data are provided with this paper.

References

1. Erb, M. & Kliebenstein, D. J. Plant secondary metabolites as defenses, regulators, and primary metabolites: the blurred functional trichotomy. *Plant Physiol.* **184**, 39–52 (2020).
2. Lacchini, E. & Goossens, A. Combinatorial control of plant specialized metabolism: mechanisms, functions, and consequences. *Annu. Rev. Cell Dev. Biol.* **36**, 291–313 (2020).
3. Colinas, M. & Goossens, A. Combinatorial transcriptional control of plant specialized metabolism. *Trends Plant Sci.* **23**, 324–336 (2018).
4. Wasternack, C. & Strnad, M. Jasmonates are signals in the biosynthesis of secondary metabolites – pathways, transcription factors and applied aspects – a brief review. *New Biotechnol.* **48**, 1–11 (2019).
5. Tholl, D. Biosynthesis and biological functions of terpenoids in plants. *Adv. Biochem. Eng. Biotechnol.* **148**, 63–106 (2015).
6. Thimmappa, R., Geisler, K., Louveau, T., O'Maille, P. & Osbourn, A. Triterpene biosynthesis in plants. *Annu. Rev. Plant Biol.* **65**, 225–257 (2014).
7. Huang, A. C. et al. A specialized metabolic network selectively modulates *Arabidopsis* root microbiota. *Science* **364**, eaau6389 (2019).
8. Pichersky, E. & Raguso, R. A. Why do plants produce so many terpenoid compounds? *New Phytol.* **220**, 692–702 (2018).
9. Sohrabi, R. et al. In planta variation of volatile biosynthesis: an alternative biosynthetic route to the formation of the pathogen-induced volatile homoterpene DMNT via triterpene degradation in *Arabidopsis* roots. *Plant Cell* **27**, 874–890 (2015).
10. Tholl, D. & Lee, S. Terpene specialized metabolism in *Arabidopsis thaliana*. *Arabidopsis Book* **9**, e0143 (2011).
11. Field, B. et al. Formation of plant metabolic gene clusters within dynamic chromosomal regions. *Proc. Natl Acad. Sci. USA* **108**, 16116–16121 (2011).
12. Field, B. & Osbourn, A. E. Metabolic diversification—independent assembly of operon-like gene clusters in different plants. *Science* **320**, 543–547 (2008).
13. Nützmann, H.-W. et al. Active and repressed biosynthetic gene clusters have spatially distinct chromosome states. *Proc. Natl Acad. Sci. USA* **117**, 13800–13809 (2020).
14. Nützmann, H.-W., Huang, A. & Osbourn, A. Plant metabolic clusters – from genetics to genomics. *New Phytol.* **211**, 771–789 (2016).
15. Bai, Y. et al. Modulation of *Arabidopsis* root growth by specialized triterpenes. *New Phytol.* **230**, 228–243 (2021).
16. Goossens, J., Fernández-Calvo, P., Schweizer, F. & Goossens, A. Jasmonates: signal transduction components and their roles in environmental stress responses. *Plant Mol. Biol.* **91**, 673–689 (2016).
17. Chini, A., Gimenez-Ibanez, S., Goossens, A. & Solano, R. Redundancy and specificity in jasmonate signalling. *Curr. Opin. Plant Biol.* **33**, 147–156 (2016).
18. Pauwels, L. et al. NINJA connects the co-repressor TOPLESS to jasmonate signalling. *Nature* **464**, 788–791 (2010).
19. Chini, A. et al. The JAZ family of repressors is the missing link in jasmonate signalling. *Nature* **448**, 666–671 (2007).
20. Fernández-Calvo, P. et al. The *Arabidopsis* bHLH transcription factors MYC3 and MYC4 are targets of JAZ repressors and act additively with MYC2 in the activation of jasmonate responses. *Plant Cell* **23**, 701–715 (2011).
21. Thines, B. et al. JAZ repressor proteins are targets of the SCF^{COI1} complex during jasmonate signalling. *Nature* **448**, 661–665 (2007).
22. Fonseca, S. et al. (+)-7-*iso*-Jasmonoyl-L-isoleucine is the endogenous bioactive jasmonate. *Nat. Chem. Biol.* **5**, 344–350 (2009).
23. Sheard, L. B. et al. Jasmonate perception by inositol-phosphate-potentiated COI1–JAZ co-receptor. *Nature* **468**, 400–405 (2010).
24. Yan, Y. et al. A downstream mediator in the growth repression limb of the jasmonate pathway. *Plant Cell* **19**, 2470–2483 (2007).
25. Gasperini, D. et al. Multilayered organization of jasmonate signalling in the regulation of root growth. *PLoS Genet.* **11**, e1005300 (2015).
26. Major, I. T. et al. Regulation of growth-defense balance by the JASMONATE ZIM-DOMAIN (JAZ)-MYC transcriptional module. *New Phytol.* **215**, 1533–1547 (2017).
27. Lorenzo, O., Chico, J. M., Sánchez-Serrano, J. J. & Solano, R. *JASMONATE-INSENSITIVE1* encodes a MYC transcription factor essential to discriminate between different jasmonate-regulated defense responses in *Arabidopsis*. *Plant Cell* **16**, 1938–1950 (2004).
28. Schweizer, F. et al. *Arabidopsis* basic helix-loop-helix transcription factors MYC2, MYC3, and MYC4 regulate glucosinolate biosynthesis, insect performance, and feeding behavior. *Plant Cell* **25**, 3117–3132 (2013).
29. Birnbaum, K. et al. A gene expression map of the *Arabidopsis* root. *Science* **302**, 1956–1960 (2003).
30. Zander, M. et al. Integrated multi-omics framework of the plant response to jasmonic acid. *Nat. Plants* **6**, 290–302 (2020).
31. Mertens, J. et al. The bHLH transcription factors TSAR1 and TSAR2 regulate triterpene saponin biosynthesis in *Medicago truncatula*. *Plant Physiol.* **170**, 194–210 (2016).
32. Van Moerkercke, A. et al. The bHLH transcription factor BIS1 controls the iridoid branch of the monoterpenoid indole alkaloid pathway in *Catharanthus roseus*. *Proc. Natl Acad. Sci. USA* **112**, 8130–8135 (2015).
33. Van Moerkercke, A. et al. A MYC2/MYC3/MYC4-dependent transcription factor network regulates water spray-responsive gene expression and jasmonate levels. *Proc. Natl Acad. Sci. USA* **116**, 23345–23356 (2019).
34. Goossens, J., Swinnen, G., Vanden Bossche, R., Pauwels, L. & Goossens, A. Change of a conserved amino acid in the MYC2 and MYC3 transcription factors leads to release of JAZ repression and increased activity. *New Phytol.* **206**, 1229–1237 (2015).
35. Kemen, A. C. et al. Investigation of triterpene synthesis and regulation in oats reveals a role for β-amyrin in determining root epidermal cell patterning. *Proc. Natl Acad. Sci. USA* **111**, 8679–8684 (2014).
36. Ohashi, Y. et al. Modulation of phospholipid signaling by GLABRA2 in root-hair pattern formation. *Science* **300**, 1427–1430 (2003).
37. Wang, S., Barron, C., Schiefelbein, J. & Chen, J. G. Distinct relationships between GLABRA2 and single-repeat R3 MYB transcription factors in the regulation of trichome and root hair patterning in *Arabidopsis*. *New Phytol.* **185**, 387–400 (2010).
38. Gualberti, G. et al. Mutations in the Dof zinc finger genes *DAG2* and *DAG1* influence with opposite effects the germination of *Arabidopsis* seeds. *Plant Cell* **14**, 1253–1263 (2002).
39. Ramachandran, V. et al. Plant-specific Dof transcription factors VASCULAR-RELATED DOF1 and VASCULAR-RELATED DOF2 regulate vascular cell differentiation and lignin biosynthesis in *Arabidopsis*. *Plant Mol. Biol.* **104**, 263–281 (2020).
40. Boccaccini, A. et al. The DOF protein DAG1 and the DELLA protein GAI cooperate in negatively regulating the *AtGA3ox1* gene. *Mol. Plant* **7**, 1486–1489 (2014).
41. Papi, M. et al. Identification and disruption of an *Arabidopsis* zinc finger gene controlling seed germination. *Genes Dev.* **14**, 28–33 (2000).

42. Gabriele, S. et al. The Dof protein DAG1 mediates PIL5 activity on seed germination by negatively regulating GA biosynthetic gene *AtGA3ox1*. *Plant J.* **61**, 312–323 (2010).
43. Zhao, H. et al. Identification and functional validation of super-enhancers in *Arabidopsis thaliana*. *Proc. Natl Acad. Sci. USA* **119**, e2215328119 (2022).
44. Baudry, A., Caboche, M. & Lepiniec, L. TT8 controls its own expression in a feedback regulation involving TTG1 and homologous MYB and bHLH factors, allowing a strong and cell-specific accumulation of flavonoids in *Arabidopsis thaliana*. *Plant J.* **46**, 768–779 (2006).
45. Ellis, C. & Turner, J. G. A conditionally fertile *coi1* allele indicates cross-talk between plant hormone signalling pathways in *Arabidopsis thaliana* seeds and young seedlings. *Planta* **215**, 549–556 (2002).
46. Xie, D.-X., Feys, B. F., James, S., Nieto-Rostro, M. & Turner, J. G. *COI1*: an *Arabidopsis* gene required for jasmonate-regulated defense and fertility. *Science* **280**, 1091–1094 (1998).
47. Haeussler, M. et al. Evaluation of off-target and on-target scoring algorithms and integration into the guide RNA selection tool CRISPOR. *Genome Biol.* **17**, 148 (2016).
48. Decaestecker, W. et al. CRISPR-TSKO: a technique for efficient mutagenesis in specific cell types, tissues, or organs in *Arabidopsis*. *Plant Cell* **31**, 2868–2887 (2019).
49. Vanden Bossche, R., Demedts, B., Vanderhaeghen, R. & Goossens, A. Transient expression assays in tobacco protoplasts. *Methods Mol. Biol.* **1011**, 227–239 (2013).
50. Wendrich, J. R. et al. Vascular transcription factors guide plant epidermal responses to limiting phosphate conditions. *Science* **370**, eaay4970 (2020).
51. Yang, B. et al. Non-cell autonomous and spatiotemporal signalling from a tissue organizer orchestrates root vascular development. *Nat. Plants* **7**, 1485–1494 (2021).
52. Lun, A. T., Bach, K. & Marioni, J. C. Pooling across cells to normalize single-cell RNA sequencing data with many zero counts. *Genome Biol.* **17**, 75 (2016).
53. McGinnis, C. S., Murrow, L. M. & Gartner, Z. J. DoubletFinder: doublet detection in single-cell RNA sequencing data using artificial nearest neighbors. *Cell Syst.* **8**, 329–337 (2019).
54. Lambert, S. A. et al. Similarity regression predicts evolution of transcription factor sequence specificity. *Nat. Genet.* **51**, 981–989 (2019).
55. Fornes, O. et al. JASPAR 2020: update of the open-access database of transcription factor binding profiles. *Nucleic Acids Res.* **48**, D87–D92 (2020).
56. Kulkarni, S. R., Vaneechoutte, D., Van de Velde, J. & Vandepoele, K. TF2Network: predicting transcription factor regulators and gene regulatory networks in *Arabidopsis* using publicly available binding site information. *Nucleic Acids Res.* **46**, e31 (2017).
57. Frith, M. C., Li, M. C. & Weng, Z. Cluster-Buster: finding dense clusters of motifs in DNA sequences. *Nucleic Acids Res.* **31**, 3666–3668 (2003).
58. Grant, C. E., Bailey, T. L. & Noble, W. S. FIMO: scanning for occurrences of a given motif. *Bioinformatics* **27**, 1017–1018 (2011).
59. Cheng, C.-Y. et al. Araport11: a complete reannotation of the *Arabidopsis thaliana* reference genome. *Plant J.* **89**, 789–804 (2017).
60. Van Bel, M. et al. PLAZA 5.0: extending the scope and power of comparative and functional genomics in plants. *Nucleic Acids Res.* **50**, D1468–D1474 (2022).
61. Kulkarni, S. R., Jones, D. M. & Vandepoele, K. Enhanced maps of transcription factor binding sites improve regulatory networks learned from accessible chromatin data. *Plant Physiol.* **181**, 412–425 (2019).

Acknowledgements

This Article was written in loving memory of A. Van Moerkercke (1979–2021). The authors thank A. Bleys for critically reading the manuscript; D. Gasperini for kindly sharing the *ProMYCs:NLS-VENUS* reporter lines, and P. Vittorioso for the *dag1* mutant, *ProDAG1:GUS* and *DAG1* over-expressing lines; J. R. Wendrich and T. Eekhout for assistance in the launching and analysis of the scRNAseq experiment; and S. Desmet and G. Goeminne from the VIB Metabolomics Core – Ghent for the thalianol profiling. This work was supported by the European Community's Seventh Framework Program (FP7/2007–2013) under grant agreement 613692-TriForC and H2020 Program under grant agreement 760331-Newcotiana to A.G.; the Special Research Fund from Ghent University to A.G. and A.R. (project BOF18/GOA/013), and M.M. (project BOF20/GOA/012); the Flemish Government (AI Research program) to Y.S.; the Research Foundation Flanders with research project grants to A.G. (G004515N and G008417N) and a postdoctoral fellowship to P.F.-C.; a Swiss National Science Foundation postdoctoral fellowship (P300PA_177831) to M.C.; and a China Scholarship Council PhD scholarship to Y.B. A.O. acknowledges funding support from the John Innes Foundation and the BBSRC Institute Strategic Program Grant 'Molecules from Nature – Products and Pathways' (BBS/E/J/000PR9790).

Author contributions

A.G., T.H.N., A.V.M., P.F.-C. and A.R. conceptualized the project. T.H.N., L.T., M.M., T.D., M.C., K. Verstaen, G.V.I., Y.S., B.D.R., K. Vandepoele, H.-W.N., A.O., A.R. and A.G. developed the methodology. T.H.N., Y.B., A.V.M., P.F.-C., L.T., T.D., M.C., G.V.I., A.R. and A.G. conducted the investigations. T.H.N., L.T., A.R., K. Verstaen and T.D. performed visualization. A.G, Y.S. and A.O. acquired funding. A.G. and A.R. administered the project. A.G., A.R., B.D.R., K. Vandepoele and Y.S. supervised the project. A.V.M., A.R. and A.G. wrote the original draft. T.H.N. and B.D.R. reviewed and edited the manuscript.

Competing interests

The authors declare no competing interests.

Additional information

Extended data is available for this paper at https://doi.org/10.1038/s41477-023-01419-8.

Supplementary information The online version contains supplementary material available at https://doi.org/10.1038/s41477-023-01419-8.

Correspondence and requests for materials should be addressed to Alain Goossens.

Peer review information *Nature Plants* thanks Yang-Dong Guo and the other, anonymous, reviewer(s) for their contribution to the peer review of this work.

https://doi.org/10.1038/s41477-023-01419-8

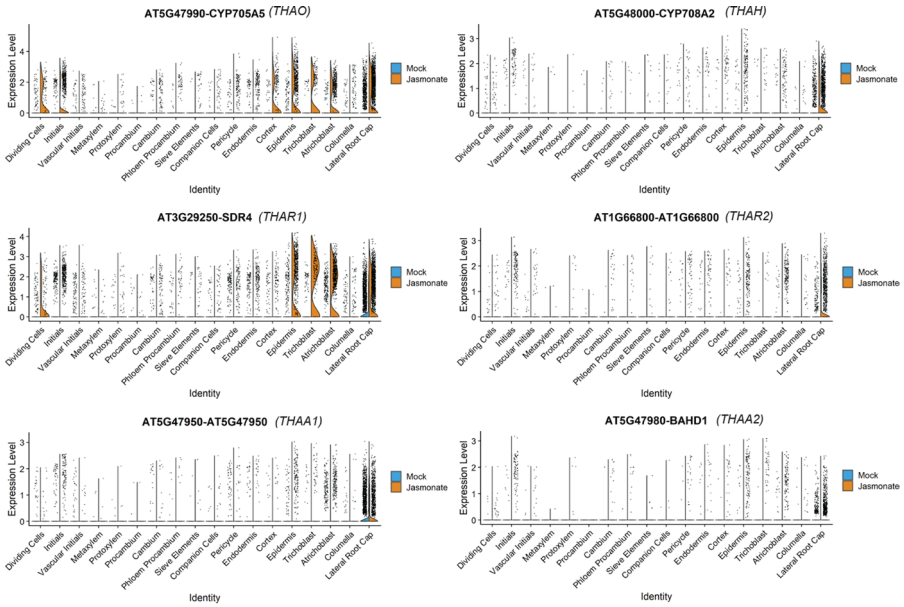

Extended Data Fig. 1 | Violin plots showing cell-specific expression of the thalianol biosynthesis genes under mock and JA treatments.

https://doi.org/10.1038/s41477-023-01419-8

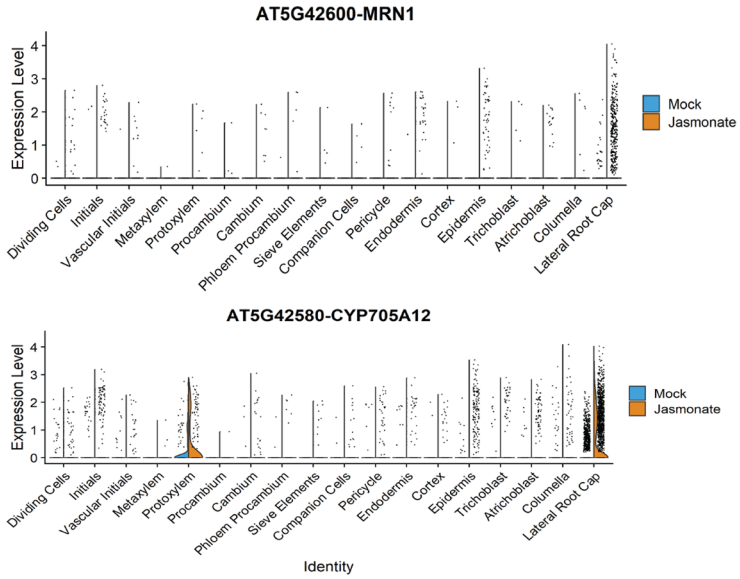

Extended Data Fig. 2 | Violin plots showing cell-specific expression of the marneral biosynthesis genes under mock and JA treatments.

https://doi.org/10.1038/s41477-023-01419-8

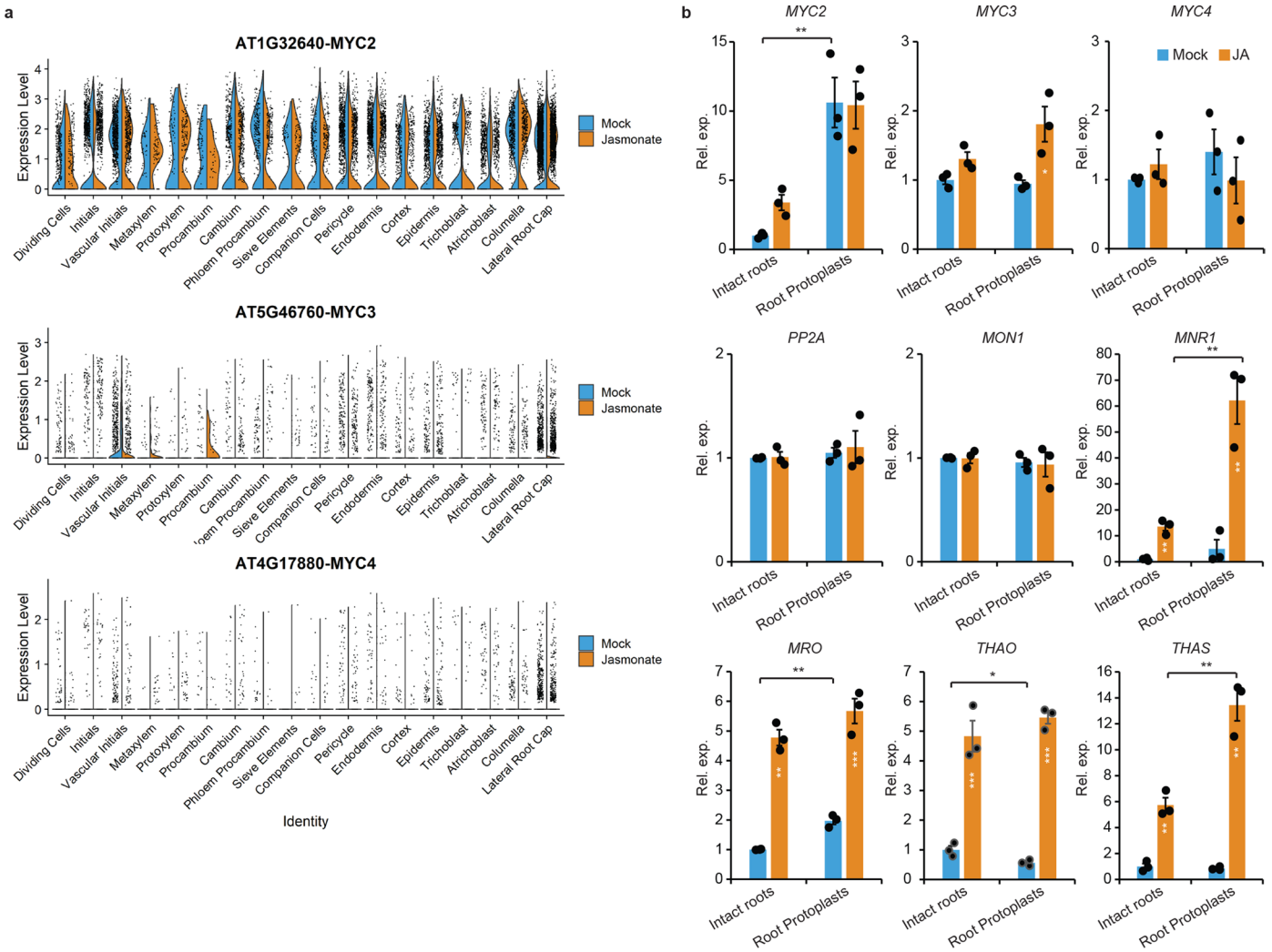

Extended Data Fig. 3 | *MYC2* expression is induced by protoplasting in root tips. a, Violin plots showing cell-specific expression of *MYC2, MYC3* and *MYC4* upon mock and JA treatments. **b**, RT-qPCR expression analysis of intact roots tips and root tip protoplasts upon mock and JA treatments. Values on the Y-axis represent fold-induction compared to mock-treated intact roots (set to 1). The error bars designate the SE of the mean (n = 3 biologically independent samples). Statistical significance was determined using the Student's *t*-test (*P < 0.05, **P < 0.005, ***P < 0.0005).

https://doi.org/10.1038/s41477-023-01419-8

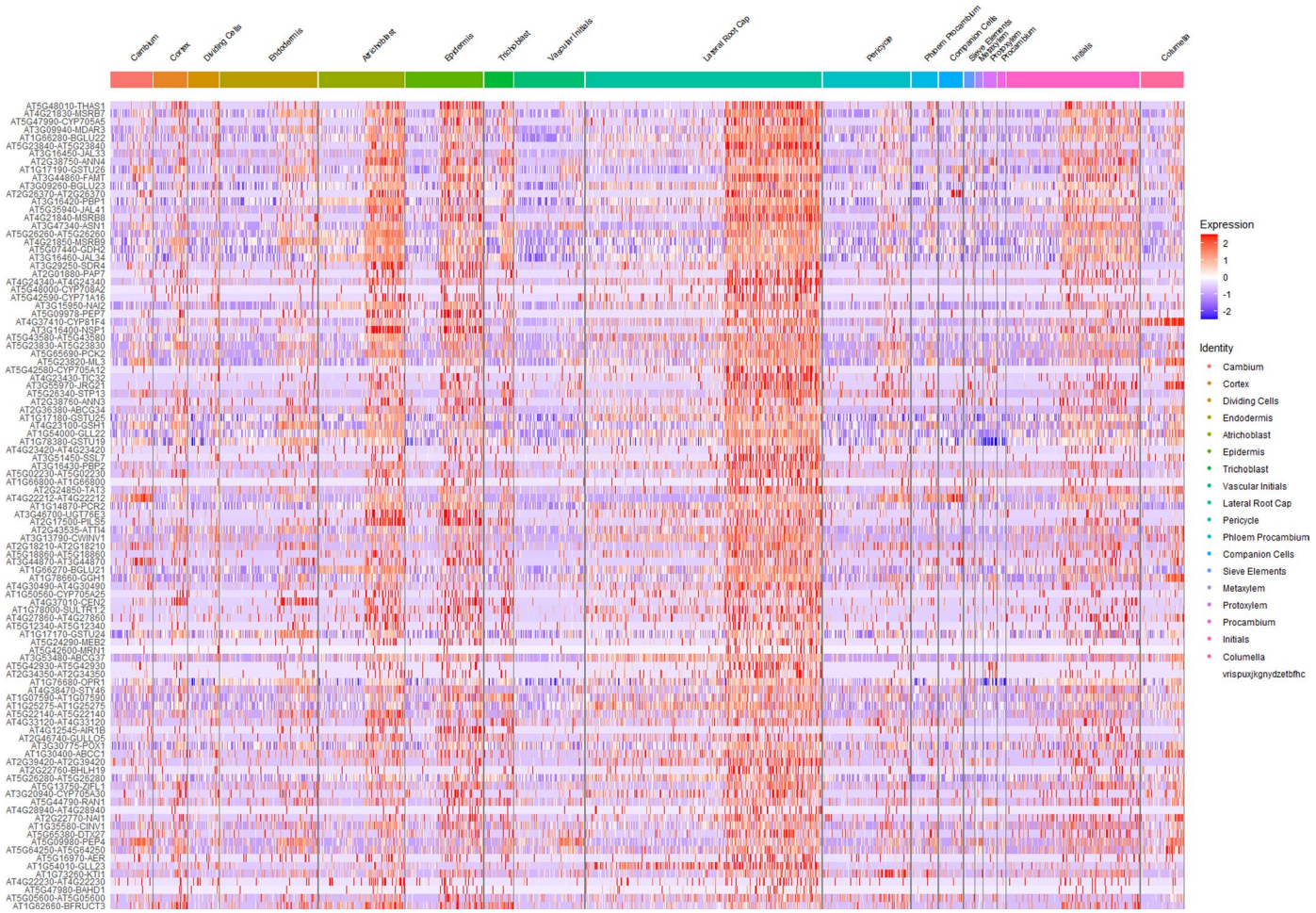

Extended Data Fig. 4 | Heatmap of *THAS* single-cell co-expression analysis. Top 100 genes co-expressed with *THAS* under JA treatment across all root tip tissue types. Expression values as log fold change of JA compared to mock conditions are shown for each of the separate tissue types.

https://doi.org/10.1038/s41477-023-01419-8

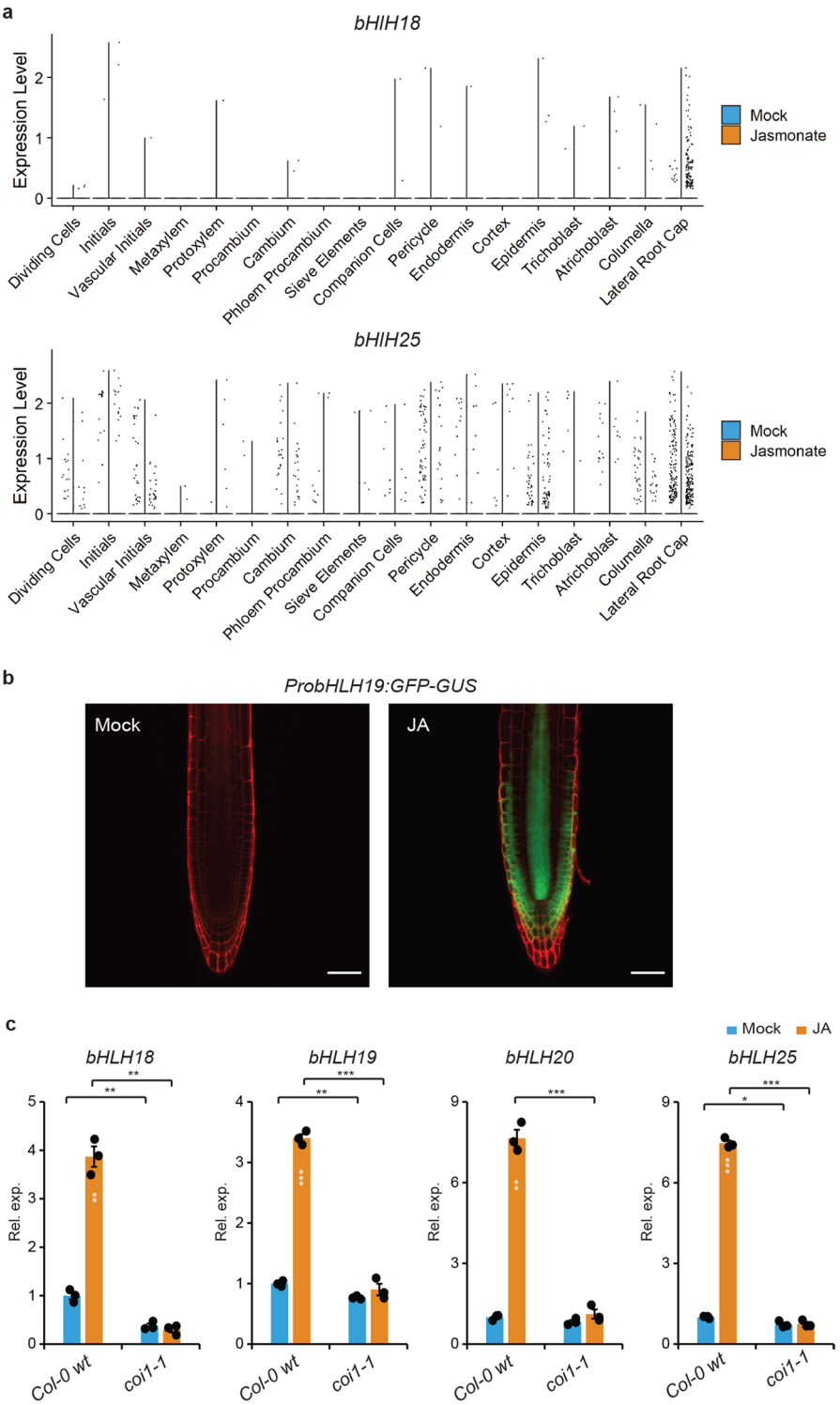

Extended Data Fig. 5 | The expression of bHLH clade IVa genes is induced by JA in a COI1-dependent manner. a, Violin plots showing cell-specific expression of *bHLH18* and *bHLH25* upon mock and JA treatments. **b**, Expression profile of *ProbHLH19:GFP-GUS* in wt root tips grown on mock or 50 µM JA for 24 h. Scale bars = 20 µm. At least 3 seedling roots were observed with similar results. **c**, RT-qPCR expression analysis of bHLH clade IV genes upon mock and JA treatments in the Col-0 wt and *coi1-1* backgrounds. The error bars designate the SE of the mean (n = 3 biologically independent samples). Values on the Y-axis represent fold-induction compared to mock-treated wt (set to 1). Statistical significance was determined using the Student's *t*-test (*P < 0.05, **P < 0.005, ***P < 0.0005).

https://doi.org/10.1038/s41477-023-01419-8

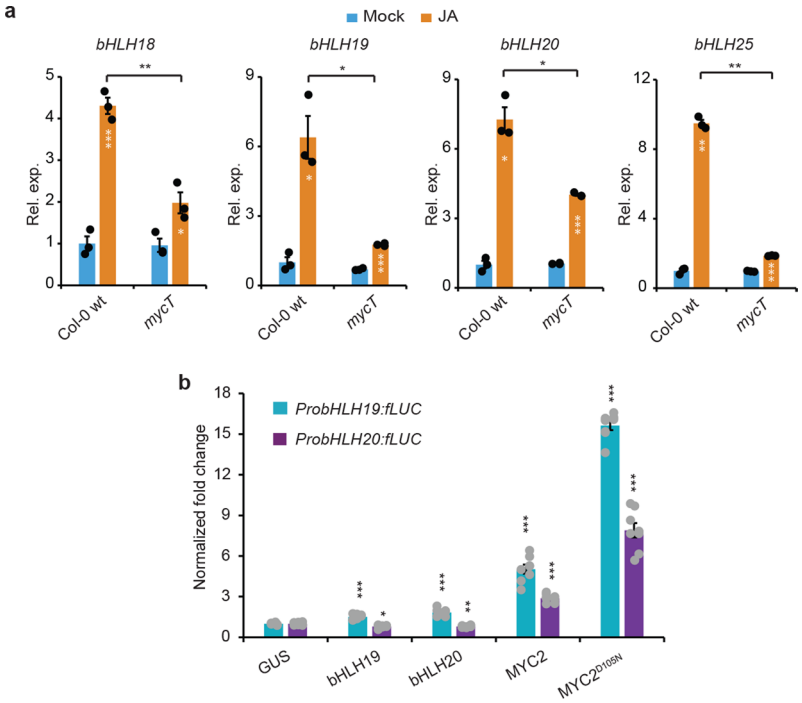

Extended Data Fig. 6 | Expression of bHLH clade IVa transcription factors is induced by MYCs. a, RT-qPCR expression analysis of bHLH clade IV genes upon mock and JA treatments in the Col-0 wt and *mycT* backgrounds. The error bars designate the SE of the mean (n = 3 biologically independent samples). Values on the Y-axis represent fold-induction compared to mock-treated wt (set to 1). Statistical significance was determined using the Student's *t*-test (*P < 0.05, **P < 0.005, ***P < 0.0005). **b**, Transactivation in *N. tabacum* protoplasts of the *ProbHLH19* and *ProbHLH20* fused to the *fLUC* reporter and cotransfected with either GUS, MYC2, MYC2^{D105N}, bHLH19 or bHLH25. Values on the Y-axis are normalized fold-changes relative to protoplasts cotransfected with the reporter constructs and a *pCaMV35S:GUS* (GUS) control plasmid (set to 1). The error bars designate the SE of the mean (n = 8 biologically independent samples). Statistical significance was determined using the Student's *t*-test (*P < 0.05, **P < 0.005, ***P < 0.0005).

https://doi.org/10.1038/s41477-023-01419-8

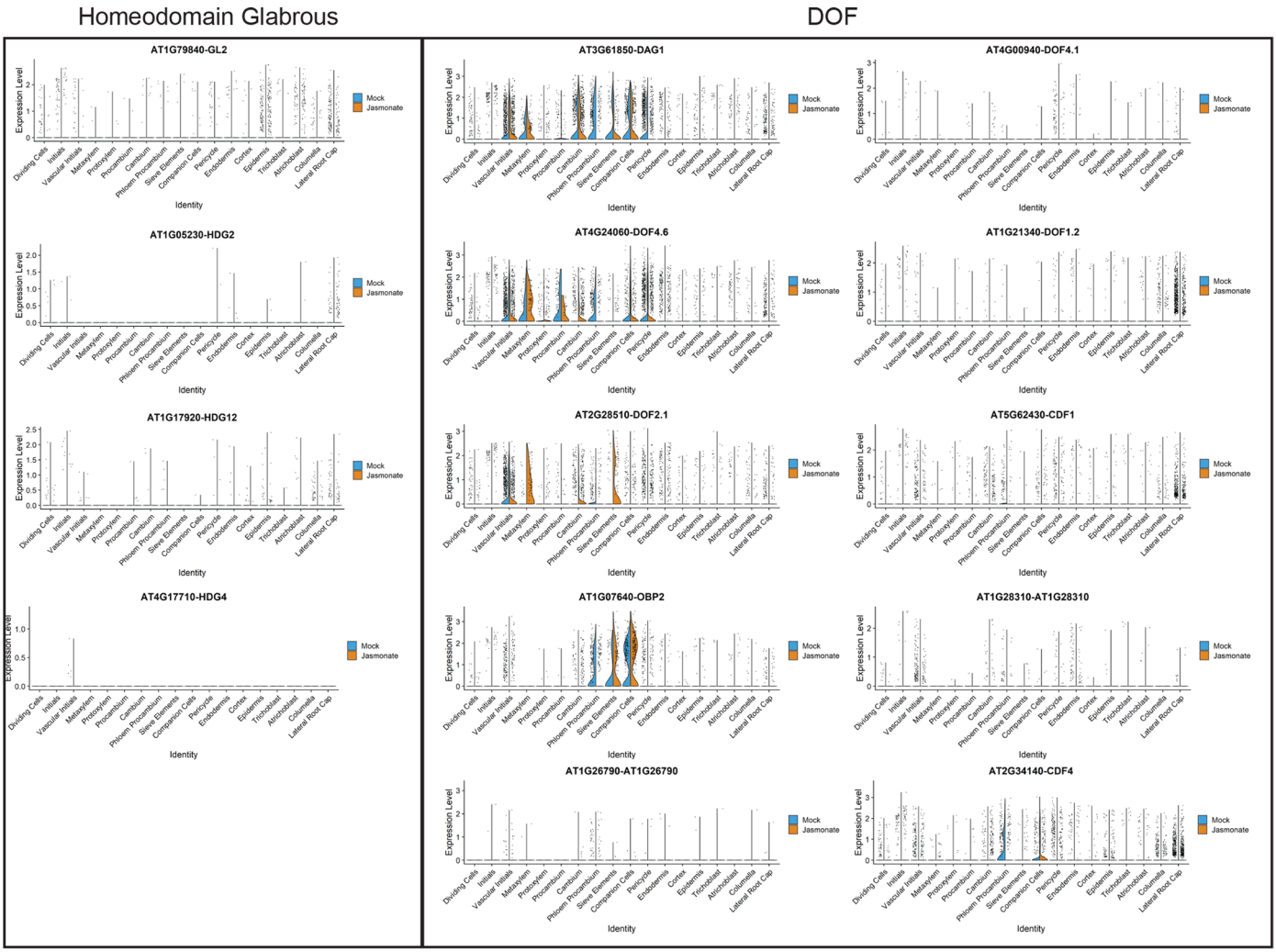

Extended Data Fig. 7 | Violin plots showing cell-specific expression of candidate root triterpene transcriptional regulators under mock- and JA-treated conditions. Only genes from the HDG- and DOF-type families that show expression in our scRNAseq dataset are represented.

https://doi.org/10.1038/s41477-023-01419-8

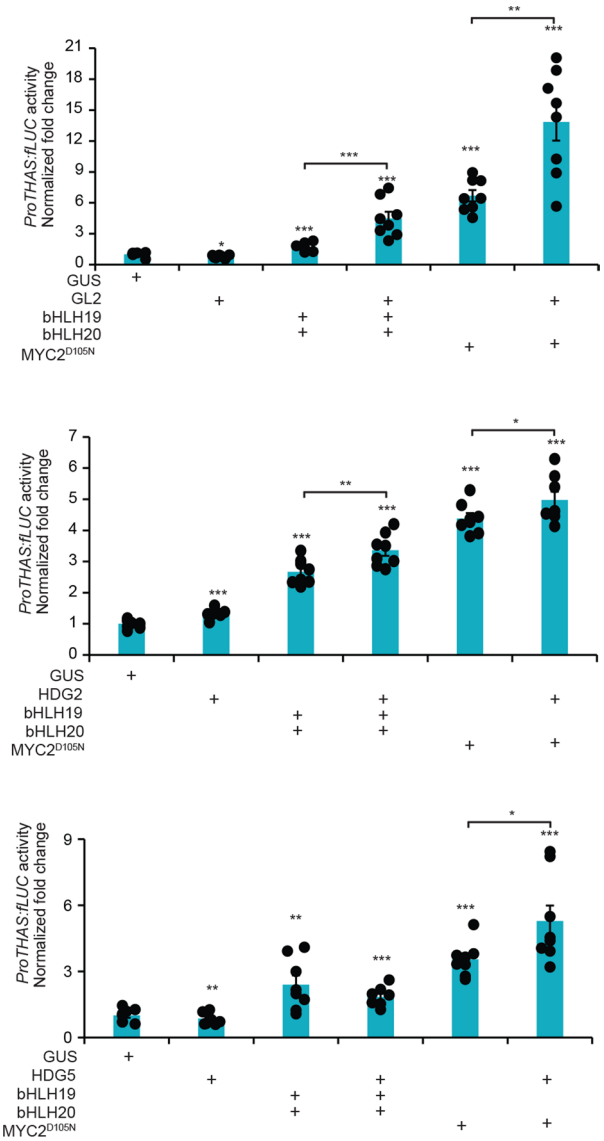

Extended Data Fig. 8 | Homeodomain glabrous proteins coactivate the transcription of the *THAS* promoter. Transactivation in *N. tabacum* protoplasts transfected with *ProTHAS* fused to the fLUC reporter, and cotransfected with combinations of GL2, HDG2, HDG5, MYC2^{D105N}, bHLH19 or/and bHLH20. Values on the Y-axis are normalized fold-changes relative to protoplasts cotransfected with the reporter constructs and a *pCaMV35S:GUS* (GUS) control plasmid (set to 1). The error bars designate the SE of the mean (n = 8 biologically independent samples). Statistical significance was determined using the Student's *t*-test (*P < 0.05, **P < 0.005, ***P < 0.0005).

https://doi.org/10.1038/s41477-023-01419-8

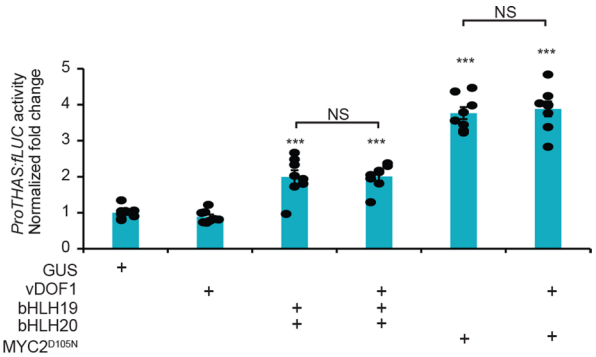

Extended Data Fig. 9 | vDOF1 proteins do not modulate transcription of the *THAS* promoter. Transactivation in transfected *N. tabacum* protoplasts of the *ProTHAS* fused to the fLUC reporter, and cotransfected with combinations of vDOF1, MYC2^{D105N}, bHLH19 or/and bHLH20. Values on the Y-axis are normalized fold-changes relative to protoplasts co-transfected with the reporter constructs and a *pCaMV35S:GUS* (GUS) control plasmid (set to 1). The error bars designate the SE of the mean (n = 8 biologically independent samples). Statistical significance was determined using the Student's *t*-test (NS, Non-significant; ***P < 0.0005).

https://doi.org/10.1038/s41477-023-01419-8

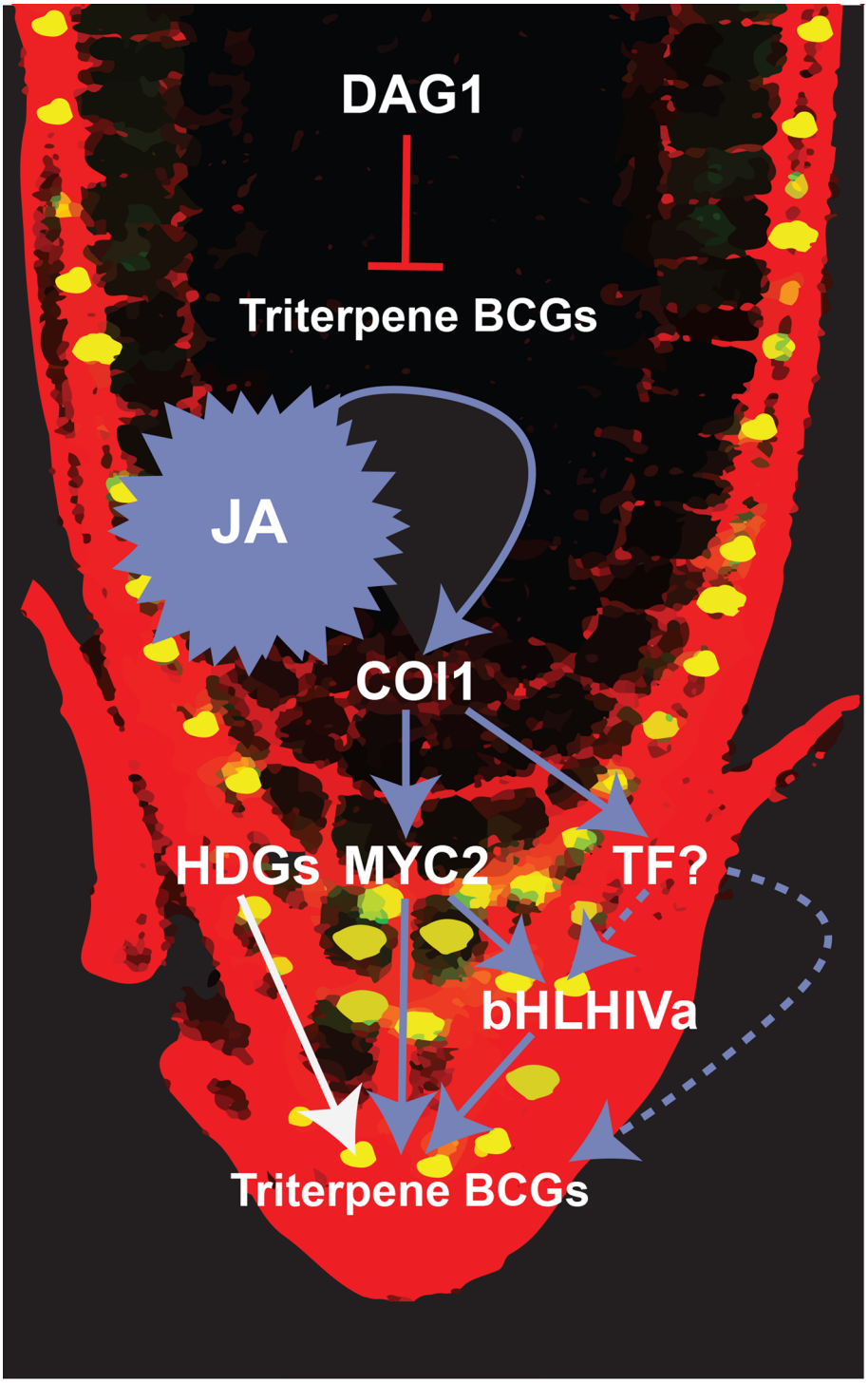

Extended Data Fig. 10 | Model for the regulatory network that drives spatiotemporal expression of thalianol and marneral biosynthesis genes in Arabidopsis root tips.

nature portfolio

Corresponding author(s): Alain Goossens

Last updated by author(s): Mar 23, 2023

Reporting Summary

Nature Portfolio wishes to improve the reproducibility of the work that we publish. This form provides structure for consistency and transparency in reporting. For further information on Nature Portfolio policies, see our Editorial Policies and the Editorial Policy Checklist.

Statistics

For all statistical analyses, confirm that the following items are present in the figure legend, table legend, main text, or Methods section.

n/a	Confirmed	
☐	☒	The exact sample size (*n*) for each experimental group/condition, given as a discrete number and unit of measurement
☐	☒	A statement on whether measurements were taken from distinct samples or whether the same sample was measured repeatedly
☐	☒	The statistical test(s) used AND whether they are one- or two-sided *Only common tests should be described solely by name; describe more complex techniques in the Methods section.*
☒	☐	A description of all covariates tested
☒	☐	A description of any assumptions or corrections, such as tests of normality and adjustment for multiple comparisons
☐	☒	A full description of the statistical parameters including central tendency (e.g. means) or other basic estimates (e.g. regression coefficient) AND variation (e.g. standard deviation) or associated estimates of uncertainty (e.g. confidence intervals)
☐	☒	For null hypothesis testing, the test statistic (e.g. *F*, *t*, *r*) with confidence intervals, effect sizes, degrees of freedom and *P* value noted *Give P values as exact values whenever suitable.*
☒	☐	For Bayesian analysis, information on the choice of priors and Markov chain Monte Carlo settings
☒	☐	For hierarchical and complex designs, identification of the appropriate level for tests and full reporting of outcomes
☒	☐	Estimates of effect sizes (e.g. Cohen's *d*, Pearson's *r*), indicating how they were calculated

Our web collection on statistics for biologists contains articles on many of the points above.

Software and code

Policy information about availability of computer code

Data collection	LightCycler480 apparatus (Roche), Zeiss LSM 710, Olympus BX51, GloMax® Navigator Microplate Luminometer, Illumina HiSeq4000, Agilent 7250 QTOF-MS
Data analysis	Demultiplexing of the raw sequencing data was done by the 10x CellRanger (version 3.1.0) software 'cellranger mkfastq'. Reads were aligned to the Arabidopsis thaliana reference genome (Ensemble TAIR10.40) using 'cellranger count', STAR 2.5.1b. All analyses were performed in R (version 4.2.0). Pre-processing of the data was done by the scater (version 1.10.1) package according to the workflow proposed by the Marioni lab (Lun et al., 2016). Potential doublets were identified using the DoubletFinder algorithm (version 2.0.0) Normalizing the raw counts, detecting highly variable genes, finding clusters and creating tSNE plots was done using the Seurat pipeline (version 3.2.3). TF motifs were mapped to a gene's regulatory regions using Cluster Buster (version compiled on Sept 2017) and FIMO (version 4.11.3). Images were then processed using Zeiss Zen 2 and ImageJ (version 1.53c) softwares. For metabolite measurement, peak areas were integrated using Masshunter Qualitative Analysis software (Agilent) (version 10.0 build 10.0.10305.0)

For manuscripts utilizing custom algorithms or software that are central to the research but not yet described in published literature, software must be made available to editors and reviewers. We strongly encourage code deposition in a community repository (e.g. GitHub). See the Nature Portfolio guidelines for submitting code & software for further information.

Data

Policy information about availability of data

All manuscripts must include a data availability statement. This statement should provide the following information, where applicable:

- Accession codes, unique identifiers, or web links for publicly available datasets
- A description of any restrictions on data availability
- For clinical datasets or third party data, please ensure that the statement adheres to our policy

The scRNAseq data are accessible via a public online browser tool (http://bioit3.irc.ugent.be/plant-sc-atlas/) and raw data are deposited at NCBI with GEO numbers GSE179820 and GSE212826, for the mock- and JA-treated root tips, respectively. All other data generated from this study are either in the main paper or the Supplementary Information. Material requests should be directed to the corresponding author. Published data for TF motifs were retrieved from the CisBP 2.00 (downloaded on Dec 2019: http://cisbp.ccbr.utoronto.ca/), and JASPAR2020 (https://jaspar.genereg.net/). The regulatory regions used for motif mapping downloaded from PLAZA Dicots 4.5 (https://bioinformatics.psb.ugent.be/plaza/versions/plaza_v4_5_dicots/).

Human research participants

Policy information about studies involving human research participants and Sex and Gender in Research.

Reporting on sex and gender	N/A
Population characteristics	N/A
Recruitment	N/A
Ethics oversight	N/A

Note that full information on the approval of the study protocol must also be provided in the manuscript.

Field-specific reporting

Please select the one below that is the best fit for your research. If you are not sure, read the appropriate sections before making your selection.

☒ Life sciences ☐ Behavioural & social sciences ☐ Ecological, evolutionary & environmental sciences

For a reference copy of the document with all sections, see nature.com/documents/nr-reporting-summary-flat.pdf

Life sciences study design

All studies must disclose on these points even when the disclosure is negative.

Sample size	Sample sizes were determined by previous pilot experiments to be sufficient to achieve desired outcomes. Sample sizes are indicated in the Figures, legends and main text.
Data exclusions	In the single-cell analysis, outlier cells were excluded when they were 4 median absolute deviations (MADs) away from the median value of either library size or numer of expressed genes. Otherwise, no data were excluded for this study.
Replication	Each experiment except the scRNA sequencing was repeated at least twice and/or with at least 3 biological repeats. Only results representing the consistent outcome are reported. ScRNA tranctiptomics was performed in a single replicate because the dataset served a gene-discovery purpose, not an atlas or specific resource to the community, and has been complemented with an extensive biological follow-up and downstream validation.
Randomization	Plant samples used in this study were genetically homogeneous and of the same age with same growth condition. Plants were randomly picked from the larger pools for experiments.
Blinding	The experiments were carried out without prior knowledge of the experimental outcome. Therefore investigators were not blinded, but biological repeats were preformed as described above.

Reporting for specific materials, systems and methods

We require information from authors about some types of materials, experimental systems and methods used in many studies. Here, indicate whether each material, system or method listed is relevant to your study. If you are not sure if a list item applies to your research, read the appropriate section before selecting a response.

Materials & experimental systems

n/a	Involved in the study
☒	☐ Antibodies
☒	☐ Eukaryotic cell lines
☒	☐ Palaeontology and archaeology
☒	☐ Animals and other organisms
☒	☐ Clinical data
☒	☐ Dual use research of concern

Methods

n/a	Involved in the study
☒	☐ ChIP-seq
☒	☐ Flow cytometry
☒	☐ MRI-based neuroimaging